



Field scale plant water relation of maize (*Zea mays*) under drought – impact of root hairs and soil texture

Helena Jorda · Mutez A. Ahmed · Mathieu Javaux ·
Andrea Carminati · Patrick Duddek · Doris Vetterlein ·
Jan Vanderborght

Received: 12 April 2022 / Accepted: 30 August 2022 / Published online: 7 September 2022
© The Author(s) 2022

Abstract

Background and aims Impact of drought on crop growth depends on soil and root hydraulic properties that determine the access of plant roots to soil water. Root hairs may increase the accessible water pool but their effect depends on soil hydraulic properties and adaptations of root systems to drought. These adaptations are difficult to investigate in pot experiments that focus on juvenile plants.

Methods A wild-type and its root hairless mutant maize (*Zea mays*) were grown in the field in loam and sand substrates during two growing seasons with a large precipitation deficit. A comprehensive dataset

of soil and plant properties and monitored variables were collected and interpreted using simulations with a mechanistic root water uptake model.

Results Total crop water use was similar in both soils and for both genotypes whereas shoot biomass was larger for the wild type than for the hairless mutant and did not differ between soils. Total final root length was larger in sand than in loam but did not differ between genotypes. Simulations showed that root systems of both genotypes and in both soils extracted all plant available soil water, which was similar for sand and loam, at a potential rate. Leaf water potentials were overestimated by the model, especially for the hairless mutant in sand substrate because the water potential drop in the rhizosphere was not considered.

Responsible Editor: Anton Wasson.

Supplementary Information The online version contains supplementary material available at <https://doi.org/10.1007/s11104-022-05685-x>.

H. Jorda · M. Javaux · J. Vanderborght (✉)
Agrosphere Institute, IBG-3, Forschungszentrum Jülich GmbH, D 52425 Jülich, Germany
e-mail: j.vanderborght@fz-juelich.de

M. A. Ahmed
Chair of Soil Physics, Bayreuth Center of Ecology and Environmental Research (BayCEER), University of Bayreuth, 95447 Bayreuth, Germany

M. A. Ahmed
Department of Land, Air and Water Resources, College of Agricultural and Environmental Sciences, University of California Davis, Davis, CA 95616, USA

A. Carminati · P. Duddek
Department of Environmental Systems Science, Physics of Soils and Terrestrial Ecosystems, Institute of Terrestrial Ecosystems, ETH Zürich, Universitätsstrasse 16, 8092 Zurich, Switzerland

D. Vetterlein
Department of Soil System Science, Helmholtz Centre for Environmental Research – UFZ, Theodor-Lieser-Strasse 4, 06120 Halle/Saale, Germany

D. Vetterlein
Soil Science, Martin-Luther-University Halle-Wittenberg, Von-Seckendorff-Platz 3, 06120 Halle/Saale, Germany

Conclusions A direct effect of root hairs on water uptake was not observed but root hairs might influence leaf water potential dependent growth.

Keywords Drought stress · Roots · Maize · Root hairs · Field scale · Model

Abbreviations

| | |
|-----------------|--------------------------------|
| CWL | Cumulative water loss |
| DAS | Day after sowing |
| ET ₀ | Reference evapotranspiration |
| ET _p | Potential evapotranspiration |
| LAI | Leaf area index |
| LWP | Leaf water potential |
| NRLD | Normalized root length density |
| PSY | Psychrometer |
| RLD | Root length density |
| RWU | Root water uptake |
| SB | Scholander bomb |
| SEM | Standard error of mean |
| WT | Wild type |
| WUE | Water use efficiency |

Introduction

Water is an important production factor for crop production and droughts are an important cause of yield declines. The increasing demand for food products in combination with prognoses of more frequent and severe droughts in the major agricultural production regions push towards practices that increase the water use efficiency. Increasing water use efficiency is a multifaceted problem involving soil, crop and irrigation management as well as the selection and breeding of drought tolerant crops. In the search for drought tolerant crops, the root system properties play an important role. The concept of root system ideotypes has been developed to identify optimal traits of root systems with respect to water uptake (Lynch 2013) and model simulations demonstrated that these optimal traits depend on soil and climate (Leitner et al. 2014; Tron et al. 2015).

Root hairs are among the traits that are discussed with regard to their function in water uptake. Root hairs, tubular extensions of epidermal cells of roots, occur in a defined zone of the root behind the elongation zone and dramatically increase the surface area available for the absorption of water and nutrients.

Although the important role of root hairs in nutrient acquisition, especially phosphate, is well accepted, their role in water uptake remains controversial. Carminati et al. (2017) made a conceptual model to evaluate the impact of root hairs on the plant water status or leaf water potential. According to this model, the impact of root hairs is expected to be larger for higher transpiration rates, lower soil water potentials, and in soils with very low soil hydraulic conductivity at lower soil water potentials, such as sandy soils. These results were confirmed in experiments with barley (Carminati et al. 2017; Segal et al. 2008), showing that root hairs facilitated root water uptake by increasing the effective root surface area for water uptake and by reducing the decline in matric potential at the root-soil interface, especially at high transpiration rates. Using the same barley genotypes in the field, Marin et al. (2021) found that under soil water deficit, root hairs enhanced plant water status and stress tolerance resulting in a less negative leaf water potential and lower leaf abscisic acid concentration. On the other hand, results from other studies did not confirm the suggested role of hairs on water uptake. Neither Dodd and Diatloff (2016) found a difference in water uptake between wild-type and mutant in barley nor Suzuki et al. (2003) found that root hairs of rice contributed to water uptake under different soil moisture conditions. For maize, Cai et al. (2021) observed no effect of root hairs on the relation between plant transpiration and either soil or leaf water potential whereas this relation was strongly dependent on the soil texture. Enhanced root length of hairless mutants might have compensated for the lack of hairs and masked their effect (Dodd and Diatloff 2016). Another reason could be that root hairs lose their function in water uptake in older roots or that they shrink and lose contact to the soil at lower soil water potentials (Duddek et al. 2022). Therefore, the role of root hairs in water uptake is not yet fully understood and seems to differ strongly depending on the soil properties, soil conditions, root system and root hair properties, and atmospheric conditions that drive the transpiration rate.

Most information on the impact of root hairs on plant water status and transpiration stems from laboratory experiments in which environmental conditions can be controlled well. The size of the soil containers has an important effect on plant growth and stress (Poorter et al. 2012) so that studies are mostly limited to juvenile plants, especially for larger crops

like maize. Variations in water content or water potential in the soil that are generated by spatially varying root water extraction, which is small in soil containers where root distributions are more uniform, are strongly reduced by capillary redistribution of water over small distances in the soil container. Hence, root distributions and soil water and soil water potential distributions can be expected to be far more homogeneous than in natural field conditions. In order to manage the experimental conditions and setup, conditions in the plant chambers are regulated and follow more regular patterns than the natural weather conditions in the field. The conditions in lab experiments are therefore not suited to investigate the role of root system properties, among which the presence of root hairs, how they adapt to environmental conditions over the entire growing season of a plant, and how they interact with the spatially variable water content and water potential in a soil profile on the plant water status and plant growth under natural field conditions.

In this contribution, we investigated how root systems of two different genotypes of a maize, one ‘wild-type B73’ (WT) and its hairless mutant (*rth3*) (Hochholdinger et al. 2008) develop in two different soil types, sand and loam, over two entire growing seasons in the field. By monitoring soil variables, i.e. soil water potentials and soil water contents, plant development, i.e. root density and leaf area index, and plant variables, i.e. transpiration and leaf water potential, during the growing season, we collected a comprehensive database that enables us to evaluate the functioning of the root systems (Novick et al. 2022). Since conditions in the field vary considerably with time and since crop development differs among treatments, the observed soil and plant variables at a certain time cannot be compared directly among treatments but must be put in context of the prevailing weather conditions and crop development. In order to link measured plant and soil variables and properties (soil hydraulic conductances, root distributions and root hydraulic properties) to root functioning, we used a mechanistic root water uptake model (Couvreur et al. 2014; Couvreur et al. 2012; Vanderborght et al. 2021) that is coupled with a soil water flow model (Cai et al. 2018b; Nguyen et al. 2022; Nguyen et al. 2020). Using this combination of monitoring data and modeling, we tested the hypothesis that the hairless mutant *rth3* experiences water stress and reduces its transpiration at less negative

soil water potentials leading to less soil water extraction, and less growth of the *rth3* mutant than of the WT, more so in the sand soil than in the loam soil. Secondly, we also tested the hypothesis that the root systems adapt to the environmental (soil) conditions and that the hairless mutant *rth3* may compensate a reduced water uptake potential by developing a more dense root system.

Material and methods

Field experiment

The soil and plant measurements performed in this study took place in the field plot experiment at the research station of Bad Lauchstädt, Germany (51°22′0″ N, 11°49′60″ E), from late April to early October in 2019 and 2020 (for details see Vetterlein et al. (2021)). During both years, the cumulative reference evapotranspiration (ET_0) exceeded cumulative rain inputs (Fig. 1). In 2019, the ET_0 [cm] for the whole season (April–September) exceeded the recorded ET_0 for the same period of time in the previous 8 years. The total rainfall over the growing period was 17.15 and 20.50 cm in 2019 and 2020, respectively. This is below the 2011–2018 average rainfall for the same months (25 cm). Looking at the water deficit, (ET_0 -Prec), this amounted to 40 cm in 2019 and 30 cm in 2020. In 2019, 1.03 cm of irrigation was applied, in 2020, 2.64 cm. Monthly average temperatures during the months of June and August in both years were slightly above the 2011–2018 means. Conversely, in both 2019 and 2020, the month of May was slightly colder than the 2011–2018 mean.

The experimental setup consists of 24 individual plots of 11×3.1 m² surface. The plots were excavated until 1 m depth; the bottom 25 cm were filled with gravel and a drainage textile was placed on top. The remaining top 75 cm of the profile were filled with two different soil substrates characterized as sand and loam, as reported in Vetterlein et al. (2021). The van Genuchten Mualem hydraulic parameters of the two substrates were characterized experimentally by Hyprop method and are provided in Table 1 (see also Fig. S1).

Two different maize (*Zea mays*) genotypes were sown in the plots: the wild-type B73 whose roots

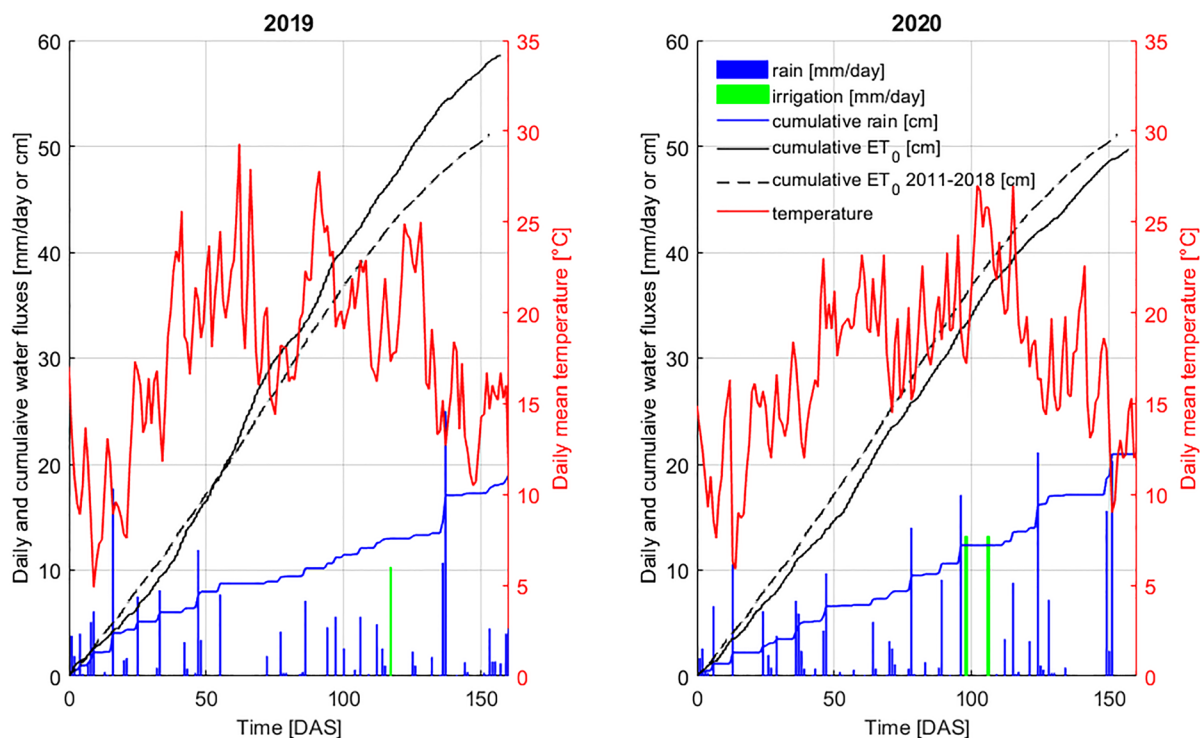


Fig. 1 Daily precipitation (rain and artificial irrigation), cumulative reference evapotranspiration (ET_0), cumulative ET_0 for 2011–2018, cumulative rain and daily mean temperature during the growing seasons in 2019 and 2020 at Bad Lauchstädt research station

Table 1 Fitted hydraulic parameters for the bimodal Mualem-van Genuchten model (Durner 1994). Table modified from Vetterlein et al. (2021)

| Parameter | Unit | Loam | Sand |
|------------|------------------------------|--------|--------|
| θ_s | $\text{cm}^3 \text{cm}^{-3}$ | 0.411 | 0.337 |
| θ_r | $\text{cm}^3 \text{cm}^{-3}$ | 0 | 0 |
| n_1 | – | 3.103 | 9.221 |
| α_1 | cm^{-1} | 0.0334 | 0.039 |
| n_2 | – | 1.108 | 1.198 |
| α_2 | cm^{-1} | 0.1670 | 0.0250 |
| w_2 | – | 0.833 | 0.321 |
| K_s | cm d^{-1} | 441 | 5 |
| τ | – | –1.089 | –0.504 |

develop root hairs (WT), and the corresponding root hair defective mutant (*rth3*) (Hochholdinger et al. 2008). Maize was sown on the 24th of April in 2019, and on the 28th and 29th of April in 2020;

harvest took place on the 8th of October in 2019, and on the 8th and 9th of October in 2020.

Four treatments were investigated (soil type X maize genotype), and each treatment was established in 6 replicate plots. On the one hand, several plant measurements such as root sampling, dry biomass and leaf area were conducted in all 24 plots at four plant developmental stages: BBCH14, BBCH19, BBCH59 and BBCH83, (Lancashire et al. 1991) corresponding to four leaves unfolded, nine leaves unfolded, end of tassel emergence and early dough, respectively (which was equivalent to 6, 9, 14 and 22 weeks after planting in 2019 and 2020). Details of sample collection are provided in Vetterlein et al. (2022).

On the other hand, soil water potential and content, transpiration flux and leaf water potential measurements were only performed in 4 of the 24 plots due to resource limitations, time constraints and the need to account for small scale variability. The latter measurements were performed on a specific area of the plot, which remained without disturbance, as indicated by Fig. 2.

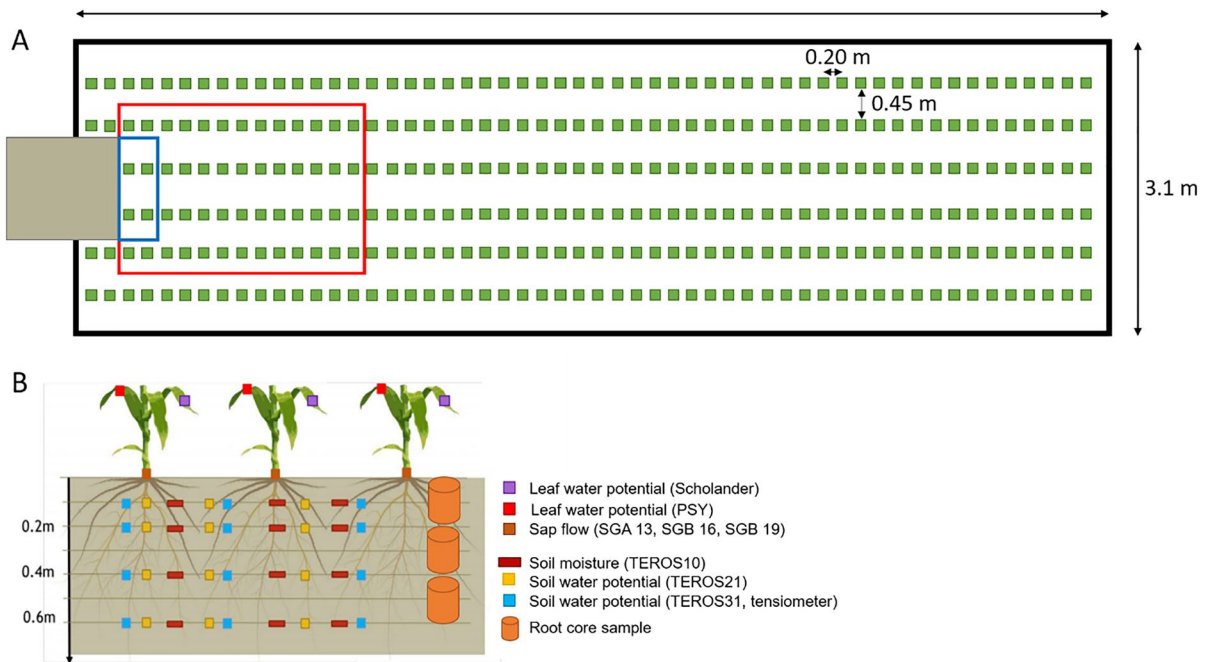


Fig. 2 **A** Plot design and dimensions. Green squares represent individual plants, the large grey rectangle indicates the location of data loggers – soil sensors were installed through the interface of the logger pit with the field plot and extend 40 to 50 cm into the plot (indicated by a blue rectangle). The red rectangle designates the area where plant measurements were performed.

B Location of the above-ground plant measurements (sap flow, and leaf water potential via Scholander bomb and psychrometers), below-ground plant measurements (root core sampling) and soil measurements (soil water content by TEROS10, and soil water potential by TEROS21 and TEROS31). Modified from Vetterlein et al. (2021)

Soil measurements

Soil water content and soil water potential measurements took place on one of the short edges of the plot (Fig. 2). TEROS 10 sensors (Meter Group AG) were used to measure soil water content every 10 minutes, and soil water potentials were measured with TEROS21 (every 5 minutes) and TEROS31 (Meter Group AG) (every 10 minutes). Three sensors of each type were placed at different positions with respect to the location of the maize plant and at four different depths (10, 20, 40 and 60 cm). Soil water potential and soil water content measurements were recorded for the whole duration of the experiment.

Plant measurements

Leaf area measurements were only performed in 2020. The leaf area of individual plants was estimated from length and width measurements of individual

leaves according to previous studies (Zhou et al. 2019):

$$LA = 0.74 \sum_{i=1}^k W_i L_i \quad (1)$$

where LA is the leaf area [L^2], k is the total number of leaves in a plant, and W_i and L_i are the maximum width and total length [L] of leaf i . The factor 0.74 accounting for the shape of the maize leaves was obtained for the specific genotypes used in this study and is the same or similar as other factors used in previous works (Mokhtarpour et al. 2010; Zhou et al. 2019). The leaf area index, or LAI, was then calculated by multiplying the mean LA by the plant density ($9.5 \text{ plants m}^{-2}$).

Dry shoot biomass measurements were performed in both 2019 and 2020. The shoots of three plants per plot were sampled according to Vetterlein et al. (2022). Root length density was determined for four growth stages in both 2019 and 2020 for three depth

intervals: 0–20 cm, 20–40 cm and 40–60 cm using soil coring as described in Vetterlein et al. (2022).

Leaf water potentials were measured via two methods. On the one hand, in-site thermocouple psychrometric sensors (PSY1, ICT International, Armidale, New South Wales, Australia) were installed on the second or third elongated leaf and left to monitor LWP until re-installation was necessary. Sensors were re-installed, on average, once a week. Psychrometers took measurements every 15–30 minutes, and were used during the months of June, July, August and September in both 2019 and 2020. Two to four sensors were installed at the same time in separate plants at each treatment plot. Insulation foam and covers were used to thermally isolate the sensors from temperature gradients during the day. On the other hand, leaf water potential measurements were also taken manually with a Scholander pressure bomb (Portable Plant Water Console model 3115, Soil moisture Equipment Corp., Santa Barbara, California, U.S.A.). Measurements were taken early morning, midday and afternoon in 2020, whereas measurements on two occasions were taken in 2019. At each measuring time, the leaves of three maize plants per plot were cut and immediately transported to the Scholander bomb for measurement.

Leaf rolling observations were taken at different times and dates during 2019 and 2020. Leaf rolling is an adaptive trait to various forms of stress, including drought stress (Baret et al. 2018; Kadioglu et al. 2012). Observations of the whole plot were categorized into 3 classes: 1 for most plants showing totally flat leaves without sign of rolling (no stress), 2 for slightly rolled leaves (medium stress) and 3 for observation of rolled leaves all over the plot (high stress).

Finally, transpiration at the plant scale was measured via sap flow sensors (Dynamax Inc., Houston, U.S.A, Campbell Scientific, Logan Utah). Dynagage heat balance sap flow sensors, of various diameters (SGA 13, SGB 16 and SGB 19) were installed on the plant stem for about two to three weeks. Due to plant growth, sap flow sensors needed reinstallation. Sensors were installed in mid-end July, and were removed in mid-September. Four technical replicates within each plot/ treatment were installed (a total of 16 sensors in the four treatments). In 2020, there was insufficient power supply to 8 sensors and thus data are only available for two treatments (loam wild-type and sand *rth3*).

Data processing and statistics

Cumulative water losses from the soil were estimated from volumetric water content measurements. Assuming that water percolation out of the soil profile could be neglected during the growing season, the cumulative water loss, CWL [L], corresponds with the cumulative evapotranspiration and was calculated using a soil water balance from the soil water storage change, ΔSWS [L], and the precipitation and irrigation according to:

$$CWL(t_i) = \Delta SWS(t_i) - \sum_{j=1}^i (P(t_j) + I(t_j)) = - \sum_{j=1}^i (E(t_j) + T(t_j)) \quad (2)$$

where $\Delta SWS(t_i)$ is the change in soil water storage between the start of the experiment and the end of day t_i , $P(t_j)$ is the precipitation and $I(t_j)$ the irrigation during day t_j , and $E(t_j)$ and $T(t_j)$ are the evaporation and transpiration during day t_j (all in length units).

A two-factorial ANOVA for factors soil type, genotype and their interaction was performed for the root-shoot ratio data in Fig. 11.

1D Hydrus simulations

The water fluxes in the soil-plant-atmosphere continuum in the experimental setup were simulated with Hydrus 1D (Šimůnek et al. 2016). Root water uptake was simulated according to Couvreur et al. (2012) as implemented in (Cai et al. 2018a). In their approach, the volume of water taken up by the root per bulk volume of soil, or otherwise known as the water sink term ($S(z)$ [T^{-1}]) is calculated as:

$$S(z) = K_{rs} (h_{T,e} - h_{T,leaf}) SUF(z) + K_{rs} (h_T(z) - h_{T,e}) SUF(z) \quad (3)$$

where K_{rs} is the root system conductance [T^{-1}], $h_{T,e}$ is the effective hydraulic head in the root zone [L], $h_{T,leaf}$ is the hydraulic head at the leaf [L], $SUF(z)$ is the standard root uptake fraction at depth z [L^{-1}], which defines the water uptake profile in a uniform water potential, and $h_T(z)$ is the hydraulic head at depth z [L]. Hydraulic heads correspond with the sum of the pressure head and elevation head, where heads are water potentials or partial potentials that express the energy or potential of water per unit weight and correspond with a length. We will use the terms head and potential as synonyms in the remainder of the

text. The first term of the sum describes root water uptake under uniform soil water potential distribution, whereas the second term describes compensatory root water uptake that results from spatially varying soil water potential distribution (Couvreur et al. 2012). A positive sink ($S > 0$) indicates water flowing from the soil into the root system, whereas a negative sink ($S < 0$) means water is released by the root system to the soil.

Transpiration is controlled by the critical leaf water potential ($h_{T,leaf\ critical}$ [L]) according to:

$$K_{rs}(h_{T,e} - h_{T,leaf}) = T_p \text{ when } h_{T,leaf} > h_{T,leaf\ critical}$$

$$K_{rs}(h_{T,e} - h_{T,leaf\ critical}) = T_{act} \text{ when } h_{T,leaf} = h_{T,leaf\ critical} \tag{4}$$

where $h_{T,leaf}$ [L] is the leaf water potential, T_p [$L\ T^{-1}$] is the potential transpiration and T_{act} [$L\ T^{-1}$] is the actual transpiration flux. The effective hydraulic head in the root zone is calculated as:

$$h_{T,e} = \int_0^{L_r} h_T(z)SUF(z)dz \tag{5}$$

where L_r [L] is the length of the root zone.

Set-up

The simulation set-up consisted of a 75 cm deep soil profile with a vertical discretization of 1 cm. A total of 22 weeks per each growing season were simulated and changes on root length density per depth interval, used to calculate root system parameterization, were updated weekly.

Boundary conditions

The reference evapotranspiration, ET_0 [$L\ T^{-1}$] was calculated according to the Penman Monteith

equation from weather data obtained at the research station. The potential evapotranspiration, ET_p [$L\ T^{-1}$], was obtained according to Allen et al. (1998):

$$ET_p = K_c ET_0 \tag{6}$$

where K_c is the crop coefficient dependent on the crop and its development stage. The K_c values used in the 2019 and 2020 simulations are summarized in Table 2. The K_c values at a certain BBCH stage were derived from an estimate of the crop cover. Data for times in between the 4 development stages was linearly interpolated in the model implementation.

The ratio of potential evaporation to evapotranspiration was obtained by using the Beer Lambert law as described in Ritchie (1972):

$$\frac{E_p}{ET_p} = e^{-k_{light} LAI} \tag{7}$$

where E_p is the potential evaporation [$L\ T^{-1}$], k_{light} is the light extinction coefficient [–], set to 0.45 based on previous studies performed on maize (Awal et al. 2006; Flenet et al. 1996). LAI was estimated from a genotype-specific relationship between shoot biomass and LAI obtained from 2020 BBCH data.

At the soil surface, we imposed a flux boundary condition corresponding to E_p or to the irrigation and rain inputs monitored at the research station when the soil water pressure head at the surface was between –16,000 and 0 cm. When the surface pressure heads reached these threshold values, a constant pressure head boundary condition was used to calculate the actual flux from the deeper soil to the soil surface (actual evaporation) or from the surface into the soil (actual infiltration). At the bottom, a seepage face boundary condition (no flux when the soil water pressure head < 0 and a constant pressure head $h = 0$ else) was chosen to represent the impact of the gravel

Table 2 Crop coefficient (K_c) values at different development stages used in the 2019 and 2020 simulations

| | 2019 | | | | | 2020 | | | | |
|--------|------|---------|-----------|---------|-----------|------|---------|-----------|---------|-----------|
| | DAS | Loam WT | Loam rth3 | Sand WT | Sand rth3 | DAS | Loam WT | Loam rth3 | Sand WT | Sand rth3 |
| BBCH14 | 42 | 1 | 1 | 1 | 1 | 43 | 1 | 1 | 1 | 1 |
| BBCH19 | 63 | 1 | 1 | 1 | 1 | 65 | 1 | 1 | 1 | 1 |
| BBCH59 | 98 | 1.2 | 1.2 | 1.2 | 1.2 | 100 | 1.08 | 1.07 | 1.07 | 1.03 |
| BBCH83 | 154 | 1.2 | 1.2 | 1.2 | 1.2 | 156 | 1.2 | 1.2 | 1.2 | 1.2 |

layer. At the plant root collar, the boundary condition switches from a flux boundary condition, equal to the potential transpiration flux, to a constant collar potential value set at $h_{T, leaf\ critical} = -16,000$ cm.

Parameterization of the root system

Both root system hydraulic parameters (K_{rs} and SUF) were estimated from RLD measurements. The SUF was assumed to be the same as the normalized RLD ($NRLD$, [L^{-1}])

$$NRLD(z) = \frac{RLD(z)}{\int_0^{L_r} RLD(z) dz} \quad (8)$$

This assumption can be made when xylem is hydraulically non-limiting and radial root hydraulic properties do not vary with depth. K_{rs} was estimated as:

$$K_{rs} = \sum_{i=1}^n RLD_i k_{rs} \Delta z_i \quad (9)$$

where RLD_i is the root length density in soil layer i [$L L^{-3}$], k_{rs} is the root system conductance normalized by the total root length below a unit of soil surface area [$L T^{-1}$] and Δz_i is the thickness of the corresponding soil layer [L]. A k_{rs} of $8.64 \cdot 10^{-6} \text{ cm d}^{-1}$ was considered based on simulations (Meunier et al. 2018b) using a root architecture model for maize and based on literature data of root segment radial and axial conductivities.

In both years, soil cores were obtained until a depth of 60 cm. However, based on experimental data from maize grown in the field, roots usually grow down to 100 cm depth. Since the RLD for the 60–75 cm interval was not measured, we estimated it to be equal to the RLD in the 40–60 cm interval in the simulations. In 2019, the RLD data obtained at the four development stages were used directly in the simulations. RLD data was linearly interpolated between the 4 measuring times. The RLD at the start of the simulation (DAS 0) was assumed to be equal to that measured at BBCH14 since simulations cannot run without any RLD data.

In 2020, the presence of dead roots from the 2019 growing season in the sand required corrections. In the loam, the 2020 RLD data were similar

to that in 2019 and samples showed no old 2019 roots. However, a larger presence of old roots was observed in the sand treatments. Thus, we estimated the degradation of 2019 old roots in the sand in order to correct the 2020 RLD data in the sand treatments.

The degradation rate at a given day i (μ_i) [T^{-1}] can be calculated as:

$$\mu_i = \mu_r Q_{10}^{\frac{T_i - T_r}{10} \circ C} \quad (10)$$

where μ_r [T^{-1}] is the reference 1st order degradation rate, and T_i and T_r are the actual and reference soil temperatures [$^{\circ}C$], respectively. The Q_{10} is the factor by which a chemical reaction rate increases with a $10^{\circ}C$ rise in temperature. In this study, Q_{10} was set to 2 [–] as this is a common value used for soil respiration in crop models (Meyer et al. 2018). First, we calculated the reference degradation rate in the 0–20 cm layer from 25th September 2019 (BBCH83) to 10th June 2020 (BBCH14) assuming the first data obtained in 2020 were made of mostly old roots. The reference 1st order degradation rate is calculated according to:

$$\mu_r = \frac{\ln\left(\frac{RLD}{RLD_0}\right)}{\Delta t \sum_{i=1}^n Q_{10}^{\frac{T_i - T_r}{10} \circ C}} \quad (11)$$

where RLD and RLD_0 are the root length densities at the end and beginning of the winter period, respectively; Δt is the time interval between day i and day $i+1$ [d]. The mean soil temperature during this time period is denominated as reference temperature (T_r), corresponding to $10.67^{\circ}C$ based on soil measurements at 10 and 20 cm depth. Once μ_r is determined, the RLD of old roots in different soil layers at day n is given by:

$$RLD_n = RLD_0 e^{\mu_r \Delta t \sum_{i=1}^n Q_{10}^{\frac{T_i - T_r}{10} \circ C}} \quad (12)$$

where T_i is the soil temperature in day i measured in the corresponding soil layer. The degradation results as well as the RLD data for both 2019 and 2020 are presented in Fig. S2.

Results

First, we present a comparison between measured and simulated data that allows us to validate the evaporation and transpiration fluxes estimated by the model, as well as the plant water status. This section also includes a comparison between water losses estimated from soil water content data and sap flow sensors. Second, both simulated and measured data are used to interpret the impact of soil substrate and maize genotype on plant-water relations.

Comparison between simulated and measured data

The evolution of the root system conductance, K_{rs} , and LAI over time in the two different growing seasons is shown in Fig. 3. K_{rs} , which was calculated from the root length density profiles, was larger in the sand than in the loam and larger for the WT than for the *rht3* mutant. Larger K_{rs} were calculated for 2020 than 2019. The LAI was similar in the loam and sand but larger for the WT than for the *rht3* mutant. The LAI development was faster in the loam than in the sand and faster in 2019 than in 2020. Figure 4 shows the volume of water in the soil estimated from soil water content measurements for each treatment and year. The horizontal grey lines indicate the water volume in the soil at the permanent wilting point, and thus the difference between the colored and grey lines shows the plant available water. Although the water volume in the loam was larger than in the sand, the amount of plant available water in the soil profile at the start of the season was similar between both substrates in both years and was about 7 to 8 cm. Thus, despite differences in water holding capacity between the two substrates, the imposed boundary condition at the bottom of the soil profile led to similar amounts of plant available water in both substrates. The plant available water in the soil profile was smaller than the reference (based on the reference ET_0) water deficit, which amounted 40 cm in 2019 and 30 cm in 2020 (see Fig. 1). As a consequence, the crop experienced drought stress during both growing seasons. At around DAS 100, the plant available water in the soil profile was almost completely consumed for all treatments so that the crop relied completely on rainfall and irrigation after DAS 100. The larger irrigation, slightly higher rainfall, and

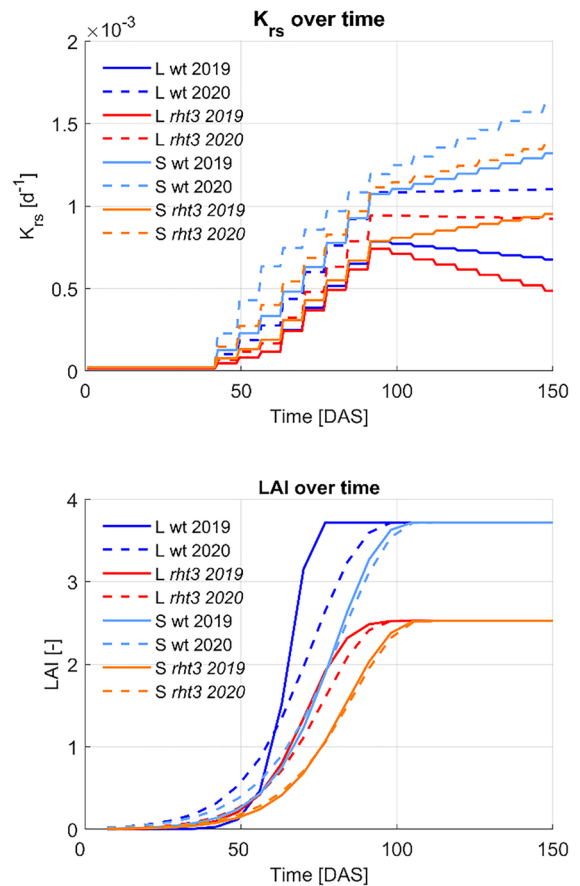


Fig. 3 Evolution of the root system conductance, K_{rs} (d^{-1}), and leaf area index, LAI, over time in the 2019 (solid lines) and 2020 (dashed lines) growing season for the different substrates (L-loam, S-sand) and genotypes (wt-wild-type, *rht3* root hairless mutant)

lower transpiration demand in 2020 resulted in wetter soil conditions after DAS 100 in 2020 than in 2019. Towards the end of the growing season, the soil profile was wetted up by rainfall events which led to apparently larger increases in water storage in the sand than in the loam soil profiles.

Simulated and measured cumulative water losses (CWL) from the soil, which correspond with the cumulative actual evapotranspiration, show an overall good agreement for all treatments and years (Fig. 5). However, according to measured data, cumulative losses were similar between treatments and differences between simulated losses in different treatments could not be confirmed by the measurements. For instance, simulations showed an earlier soil water

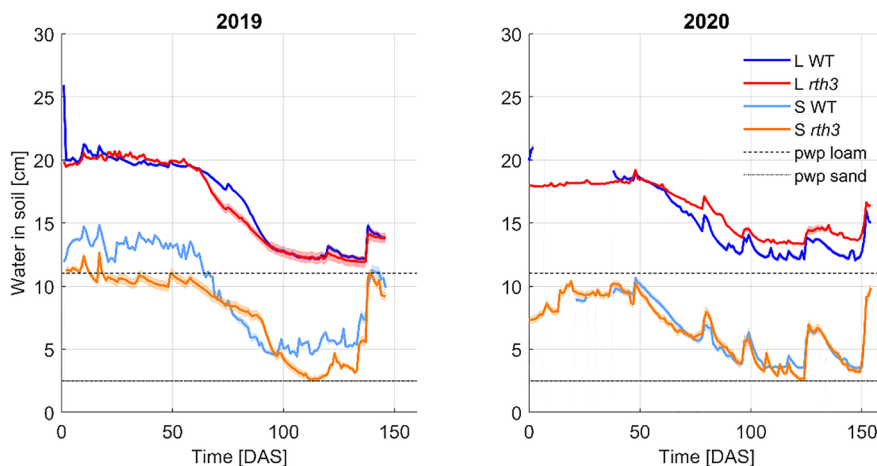


Fig. 4 Water in the soil profile [cm] estimated from water content measurements for the different substrates (L-loam, S-sand) and genotypes (wt-wild-type, *rht3* root hairless mutant). The solid colored lines indicate the mean values, whereas the

shaded areas denote the standard error of the mean (SEM). The solid and dotted grey lines denote the water remaining in the soil at the permanent wilting point calculated from the water retention curves of the loam (L) and sand (S), respectively

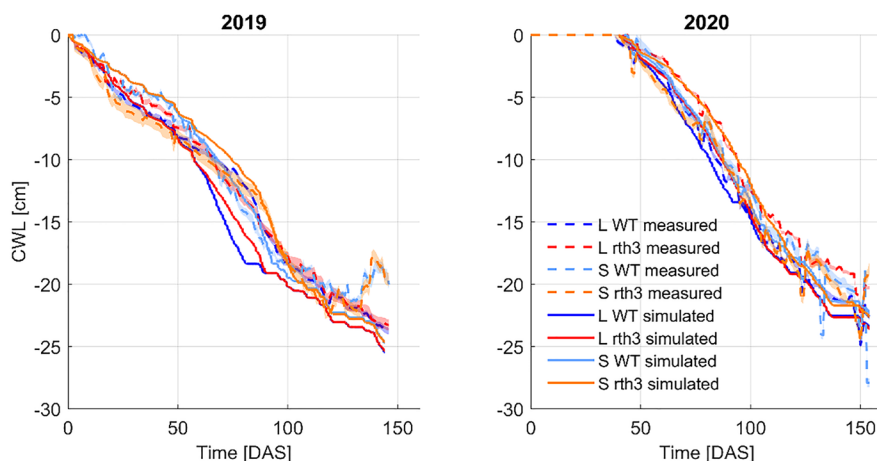


Fig. 5 Simulated (solid lines) and measured cumulative (dashed lines) water losses (CWL) from the soil in 2019 and 2020 for the different substrates (L-loam, S-sand) and genotypes (WT-wild-type, *rht3* root hairless mutant). Measured losses are computed based on a water balance derived from

water content measurements. Simulated losses correspond to the sum of evaporation and transpiration fluxes. Lines indicate mean values, whereas shaded areas denotes the standard error of the mean (SEM)

loss in the loam than in the sand in 2019 but this was not confirmed by the measurements (Fig. 5).

There are times at which the measured CLW increased (see sand treatments in 2019), which would mean that the increase in water content in the soil was larger than the amount of precipitation. This is not possible since lateral and upward flow are restricted in the field plots. However, this artifact could be caused by the location of

the water sensors in preferential flow pathways where a larger increase in water content is measured than in the average soil volume. This artifact was most significant in the sand treatments, where unstable flow may occur caused by different processes such as textural layering, air entrapment, water repellency or unstable wetting (Hendrickx and Flury 2001). The artifact implies that the average of the soil moisture measurements may deviate

much more from the average water content in the plot than the standard errors of the mean of the sensor measurements, which assumes uncorrelated and independent sensor measurements, suggest.

The model relies on estimates of potential evapotranspiration from meteorological data and plant development (K_c factors) and it predicts how evaporation and transpiration are reduced (or downregulated) when the soil water content decreases. The dependence on soil water content differs between both processes with soil evaporation depending mainly on the water content of a thin surface layer and transpiration depending on the water content in the entire root zone. The comparison between measured and simulated cumulative soil water losses allow us to validate the estimations of evapotranspiration. During the first 50 days after sowing, LAI was low and most water was lost via soil evaporation. The water lost by evaporation was compensated by precipitation so that the soil water storage did not decrease over time (Fig. 4, data only available for 2019). The potential evaporation during this period (17 cm) was larger than the actual water loss due to evaporation (7 cm) and the simulation model reproduced the downregulation of the soil evaporation when the soil surface dries out accurately. After 50 DAS, LAI increased substantially and transpiration and root water uptake became more important than evaporation. Roots can extract water from the whole soil profile, which led to a drying out of the soil (Fig. 4). The simulations reproduce also the cumulative water losses after DAS 50 (Fig. 5), which were mainly caused by plant transpiration. Sap flow measurements correspond with root water uptake and plant transpiration and are additional information that can be used to validate the simulated crop transpiration. Figure 6 shows the sap flow measurements for the different treatments together with the simulated transpiration, the measured soil water losses, and the simulated evapotranspiration for the time periods that sap flow data were available (roughly after DAS 75). Taking into account the relatively large uncertainty of the sap flow measurements due to between plant variability, the transpiration derived from sap flow measurements is consistent with the evapotranspiration derived from water balance measurements, with the exception of the sand wild-type treatment in 2019 where the sap flow measurements seem to overestimate the water loss from the plot

considerably (Fig. 6). The good agreement between sap flow measured transpiration and the evapotranspiration derived from the water balances (except for the sand wild-type treatment in 2019) supports simulated results, which predicted that the largest fraction of evapotranspiration losses comes from crop transpiration during this time period. Due to its lower LAI, this simulated fraction was a bit lower for the *rth3* mutant. However, the precision of sap flow measurements was neither high enough to differentiate evaporation from evapotranspiration fluxes nor to differentiate between different treatments.

The model simulates lower transpiration fluxes than the sap flow measurements in the loam treatments in 2019 (both WT and *rth3*), whereas simulated and measured transpiration fluxes match for the sand *rth3* treatment in 2019 and 2020 and for the loam WT in 2020. In both years, we can also observe that for some periods, while the measurements show an increase in cumulative transpiration, the model predicts no transpiration flux, which is later resumed once water becomes available in the soil. Examples of these disagreements between measured and simulated transpiration can be seen in 2019 between 120 and 125 DAS, as well as between 128 and 134 in all treatments, and between 92 and 97 DAS in 2020 for the loam wild-type treatment (Fig. 6).

Figure 7 shows simulated and measured leaf water potentials (LWP) with psychrometers (PSY), and an assessment of the plant water stress based on appearance or presence of rolled leaves. A comparison between LWPs measured by the psychrometers and the Scholander bomb (SB) method in Fig. S3 shows that both measurements are consistent with each other with PSY measuring less negative LWPs than the SB. Considering that the model simulates plant stress when the critical LWP (-1.6 MPa) is reached, the times when the model simulated stress seem to match with observations of rolled leaves. In 2019, rolled leaves appeared in the loam soil at around DAS 90 which is consistent with the simulated drop in LWP around that time. At the time stress became apparent in the loam soils, no rolled leaves were observed in the sand yet, which is consistent with the simulated LWPs which dropped around 10 days later in the sand. In 2020, rolled leaves were observed at the same times in all treatments except for the *rth3* mutant in the sand, which showed a later appearance of rolled leaves. This was consistent with the

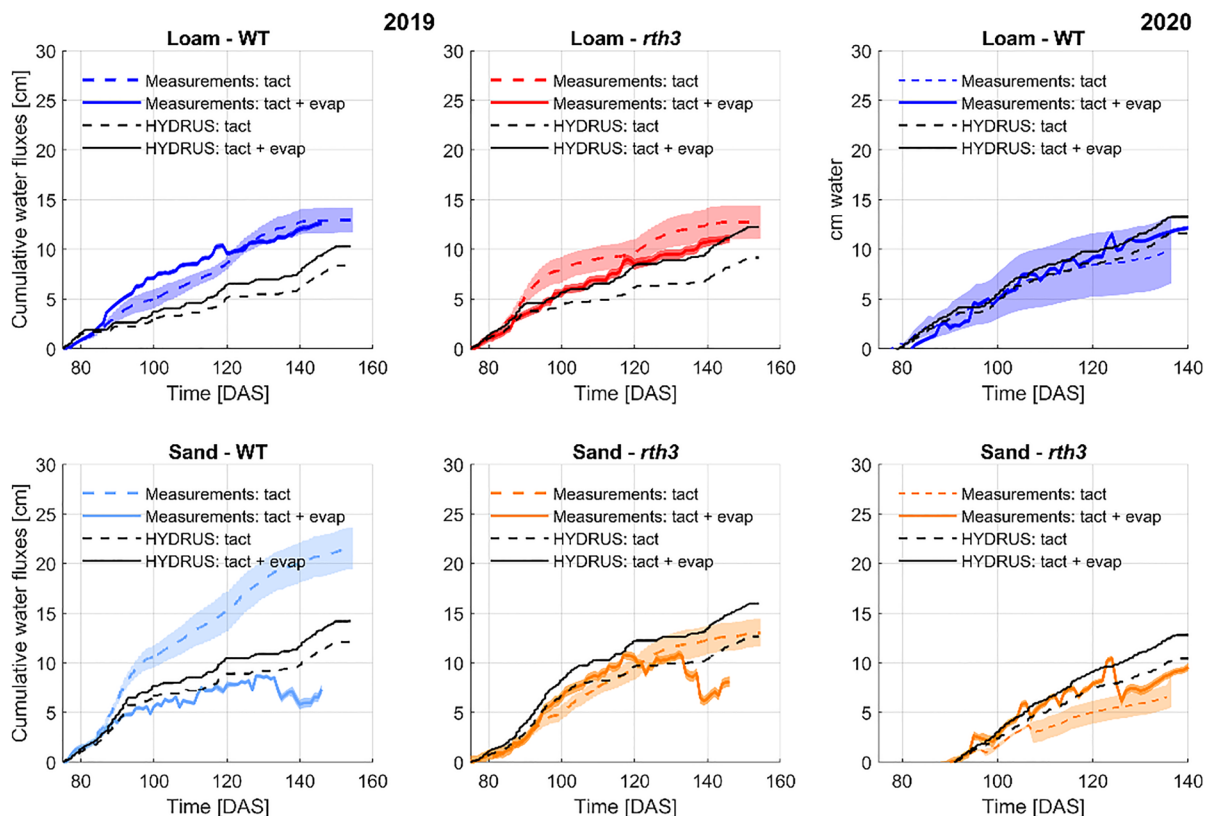


Fig. 6 Simulated (black lines) and measured (colored lines) cumulative transpiration (dashed lines) and evapotranspiration (solid lines) during sap flow measurements for 2019 and 2020. Regarding the measured data, lines denote mean values,

whereas the shaded area depicts the standard error of the mean (SEM). Light and dark shaded areas refer to the SEM of measured transpiration and evapotranspiration, respectively

simulated LWPs which dropped later in this treatment. Regarding LWP measured with PSY, these measurements show values that fall below the -1.6 MPa threshold value defined in the model.

A larger data set of measured LWP is available in 2020 and PSY LWPs did not drop to such low values as in 2019, probably due to the lower potential transpiration or atmospheric demand for water in 2020 than in 2019. During times when the model simulates LWPs above the stress threshold value of -1.6 MPa, the PSY measured leaf water potentials were lower than the simulated ones and more so in the sand than in the loam and for the *rth3* mutant than for the WT (Fig. 8).

Setting the threshold LWP, $h_{T, leaf\ critical}$, at which the model switches to a constant LWP potential and starts reducing transpiration, to -2 MPa led to a slight improvement in the agreement between

measured and simulated LWP (see Fig. S4). However, this had little to no impact on the timing of the onset of stress nor on the transpiration fluxes. This shows that the model is able to predict the water dynamics in the soil and crop and the occurrence of low leaf water potentials causing leaf rolling but was not able to model plant water potentials accurately in the time period before plant transpiration reduced due to water stress. Since the model simulations provide a continuous dataset of water fluxes and water potentials for all treatments throughout the whole growing season and provide a dataset that is consistent with weather conditions and crop development, which differ between years and treatments, we base the comparison among treatments on the model simulations.

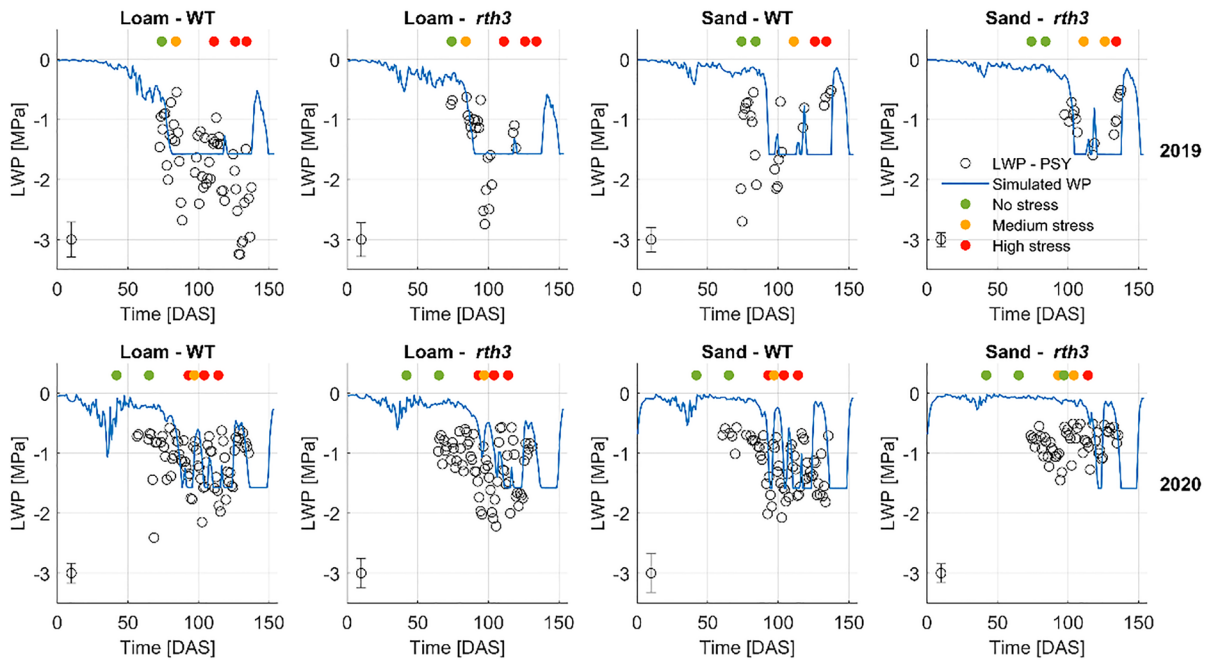


Fig. 7 Simulated and measured leaf water potential (LWP) and qualitative stress level at midday derived from leaf rolling observations. Qualitative stress levels are indicated at 74, 84, 111, 126 and 134 DAP in 2019, and 42, 65, 93, 97, 104 and

114 DAP in 2020. The vertical bars in the bottom left corners of the plot represent a LWP measurement \pm the standard error of the mean

Comparison among treatments

Figure 9 shows the cumulative potential transpiration, actual transpiration and evaporation fluxes simulated by the model. The values displayed in the figure indicate the times when the actual transpiration deviates from the potential transpiration, thus the onset of stress. For the sand WT, the onset of stress is simulated more or less at the same time in both years. For the other treatments, simulations predict an earlier onset of stress in 2019 than in 2020 (Fig. 9). This is difficult to confirm with rolled leaves observations (Fig. 7) since we did not carry out observations at the same times in both years.

The model predicts that stress occurred earlier in loam than sand treatments in both years. This is supported by rolled leaves observations in 2019, and in 2020 for the *rth3* mutant. The predicted earlier onset of stress in the loam treatments is linked to the faster development of the shoot biomass in this substrate (see Vetterlein et al. (2022) and LAI in Fig. 3).

Figure 9 shows that evaporation was the main driver for water loss from the soil during the first 50 days of the growing season. Total evaporation

losses were quite large in all treatments, ranging from half the amount of water transpired by the plant to about the same amount. With respect to soil type, evaporation losses were larger in the loam than in the sand in both years.

Potential transpiration, estimated from LAI and reference evapotranspiration (ET_0) using Kc factors was larger for the WT than for the mutant *rth3* in both years (Fig. 9). The faster shoot development and faster increase of LAI and larger final LAI were the underlying causes of the larger potential transpiration of the WT compared to the *rth3* mutant. Smaller differences in potential transpiration were simulated between soil substrates, with plants growing faster in the loam than in the sand. Larger potential transpiration was simulated in 2019 than in 2020 (Fig. 9) due to a larger reference ET_0 (Fig. 1). In both 2019 and 2020, discoloration in the sand substrate early in the season (BBCH14~45 DAP), indicated P deficiency. This is supported by measurements of P in leaves (Vetterlein et al. 2022). Figure 4 shows high plant available water in the soil up until 45 DAS in all treatments. Thus, early differences between the

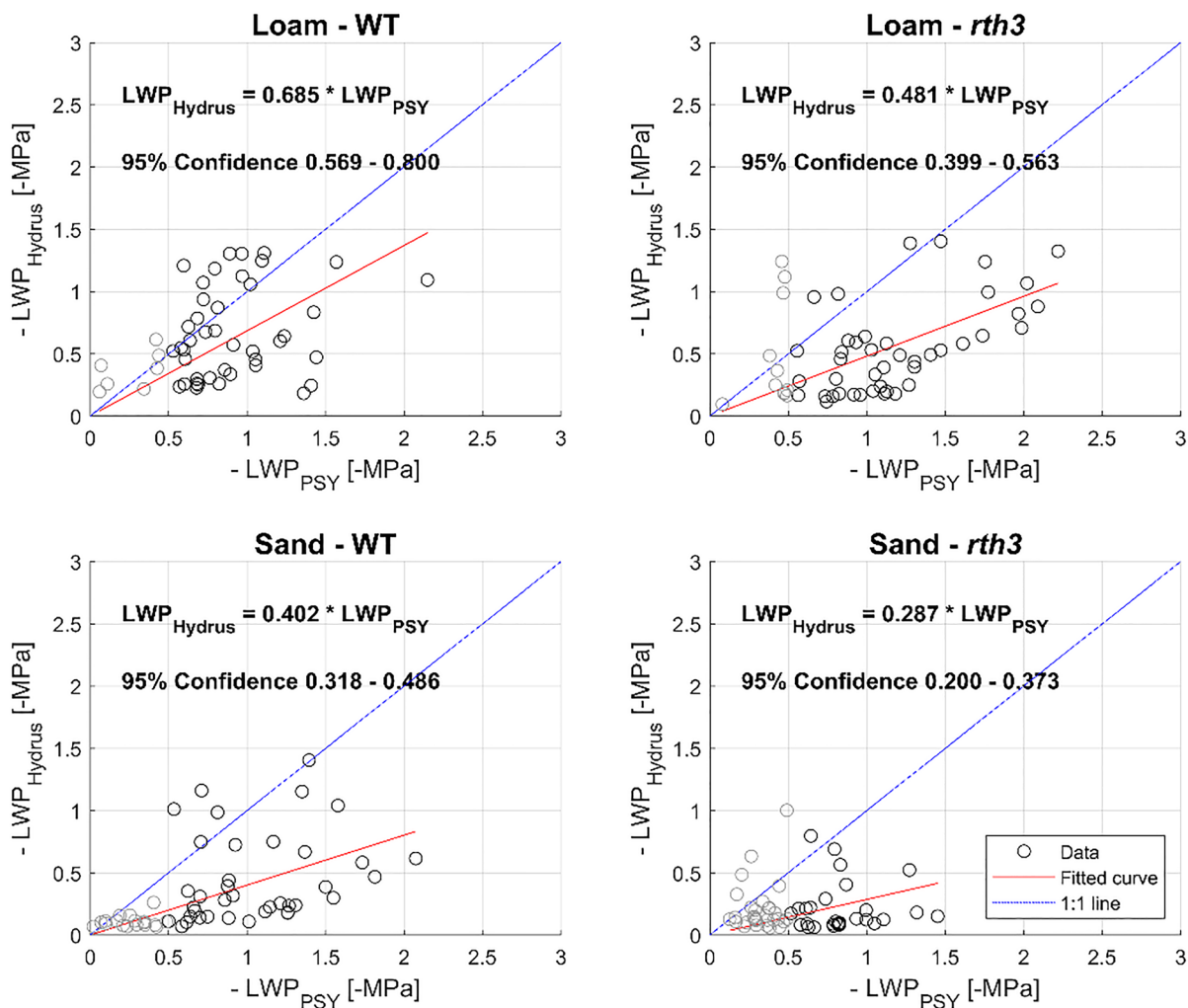


Fig. 8 Comparison between simulated and measured leaf water potential at midday during the 2020 growing season when the simulated LWPs were above the critical threshold value $h_{T, leaf\ critical} = -1.6$ MPa. Red lines represent a linear fit through the origin. Measurements of LWP larger than

-0.5 were included. Even though the psychrometer measurements above -0.5 MPa are not precise, they provide information about the leaf water status and indicate that the leaf water potentials are high (these are plotted as grey dots)

development in the two soils are not due to reduction in plant water uptake and transpiration.

The differences in potential transpiration between the different soils, genotypes and years reflect the impact of the crop development and the climatic conditions on the water demand by the crop. Looking at the simulated actual water uptake or transpiration by the crop, it seems that these differences in demand are not followed by differences in actual uptake. In the loam, despite larger potential transpiration in 2019 than in 2020, the model predicts larger actual

transpiration in 2020. In 2019, plants relied on less rain and only one irrigation event. In contrast, in 2020 rain inputs were larger and the plots were irrigated twice (Fig. 1). The simulated actual transpiration was closer to the potential transpiration in 2020 than in 2019, suggesting that plants suffered less from water stress in 2020 than in 2019. Despite the larger potential transpiration of the WT than the *rth3* mutant, due to a difference in growth and shoot development, the simulated actual transpiration by both genotypes was

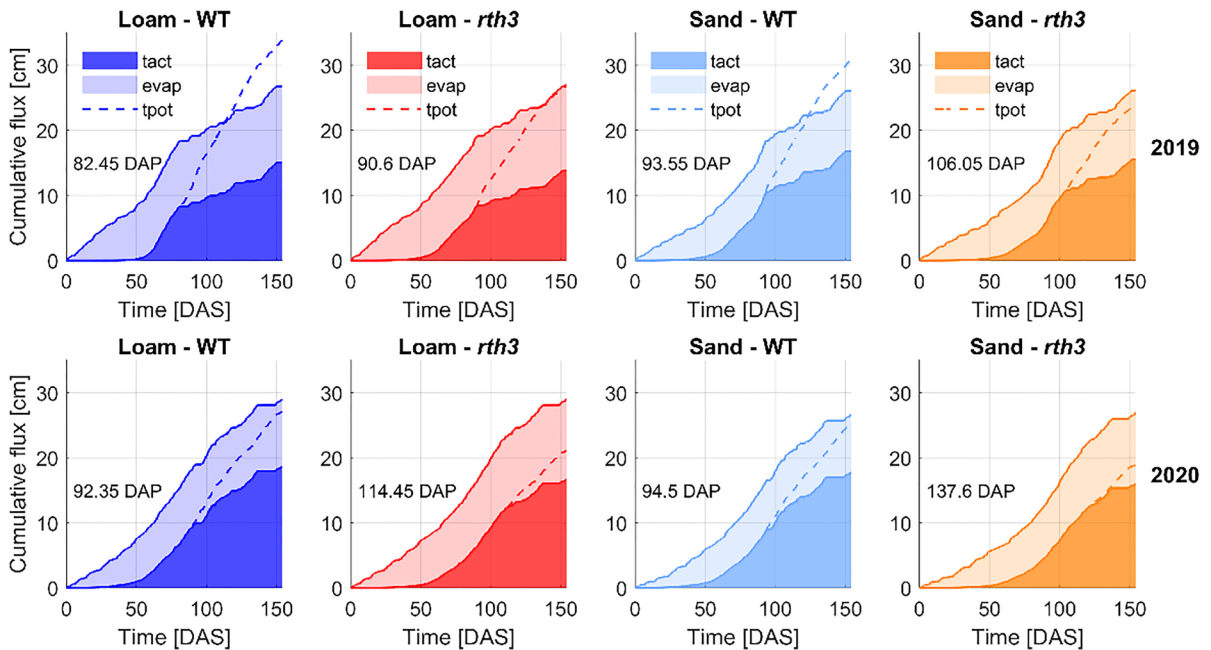


Fig. 9 Simulated cumulative fluxes for 2019 and 2020 growing seasons. Actual transpiration fluxes (t_{act}) are depicted in dark colored areas, evaporation fluxes (evap) in light colored

areas, and potential transpiration fluxes (t_{pot}) in dashed line. The time at which t_{act} deviates from t_{pot} , i.e. the onset of stress, is indicated on the plot

similar in 2020 and even slightly higher for the *rth3* mutant than for the WT in 2019.

The similar or even larger simulated actual transpiration by the *rth3* mutant than by the WT together with a lower shoot biomass of the *rth3* mutant is obviously translated in a lower water use efficiency (WUE) of the mutant (Fig. 10). In the loam, the WUEs tend to decrease with time whereas they increase or remain constant over time in the sand. At BBCH83, no systematic soil type effect on the WUE can be observed. It should be noted that WUEs were calculated based on simulated transpiration and the measured shoot biomass. When evaporation losses are added to the transpiration losses, the WUEs are roughly halved and they are the smallest at the beginning of the growing season when evaporation is the largest share of evapotranspiration. Looking at the root-shoot ratio (Fig. 11), there is clear soil type effect with a higher root-shoot ratio in the sand than in the loam. Generally, larger root-shoot ratios were observed for the *rth3* mutant than for the WT, although this tendency was found to be not significant. The genotype differences in WUE can therefore at first sight not be explained by differences in root development that was expressed in terms

of total root length. A more detailed evaluation of WUE should include the actual root biomass instead of the root length and also root exudation. Thicker roots were observed in the sand than in the loam which would amplify the observed soil type effect on root-shoot ratios.

Despite differences in root development in different soils and differences in WUE between the two genotypes, simulation results indicated that plants did not experience water stress in any treatment until the plant available water was close to 0 (Fig. 12). Figure 12 shows the simulated hourly ratio of actual to potential transpiration (i.e. stress) as a function of the simulated plant available water content in the soil. This figure shows that the root system, regardless of soil type or genotype, was very effective in taking up water. We observed that once plants emptied the soil from water and reached stress, transpiration relied on water supplied by irrigation or rain events.

Finally, Figs. 13 and 14 display the simulated water volume extracted per volume of bulk soil per day (water sink) at midday and midnight, respectively. Data are only presented for the loam WT treatment (data for all treatments can be found in the

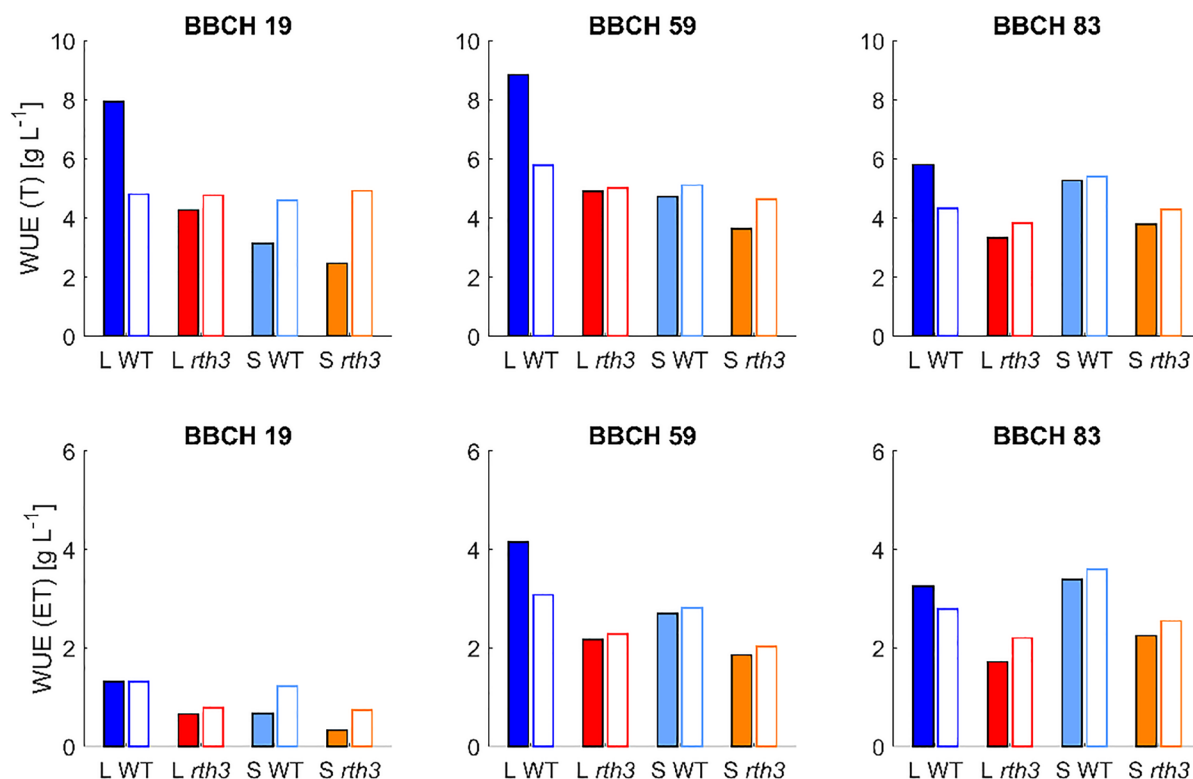


Fig. 10 Impact of substrate (loam - L, sand - S) and maize genotype (wild-type—WT, root hair mutant *rth3*) on water use efficiency (WUE) at different stages of plant development (BBCH 14, BBCH 19, BBCH 59 and BBCH 83) in the first (2019 – colored bars) and second (2020 – white bars)

year. Cumulative transpiration and evaporation per plant were obtained from simulations, while dry shoot biomass was obtained from field measured data. WUE is provided for transpiration (T) and for evapotranspiration (ET)

Supplementary material, Figs. S5 and S6). A positive sink indicates water flowing from the soil into the root system, whereas a negative sink denotes a flow from the root to the soil. Due to later arrival of roots in the deeper soil layer, the RWU starts first in the upper soil layers. In 2020, RWU in lower layers started earlier than in 2019 due to the earlier presence of roots (Fig. 13). However, since we did not sample below 40 cm at BBCH19 in 2019, we might have underestimated the presence of roots deeper in the soil at the beginning of the growing season. Also after 100 DAS, when the root system was almost completely developed, the model simulates that RWU after an irrigation or rainfall event starts first in the upper layer whereas it resumes later deeper in the soil profile. In both 2019 and 2020, the model simulates water redistribution via the root system. Early in the season in both years, we simulate hydraulic lift, i.e. water redistribution via the root

system from bottom layers towards the top during night, (Fig. 14). Later in the season, once the soil gets depleted of water, water redistribution from top layers to the bottom is simulated after rain or irrigation (Fig. 14). The water released to the soil in the bottom layer is later taken up by the plants. Between 50 and 80 DAS, the simulated volume of water redistributed via the root system in the loam treatments amounted to 10–15% of the volume of water transpired, whereas in the sand treatments the ratio was about 20–25%. Simulated water redistribution from 80 to 110 DAS ranged from 30 to 40% of the transpired water in the WT treatments, to 20–30% in the *rth3* treatments.

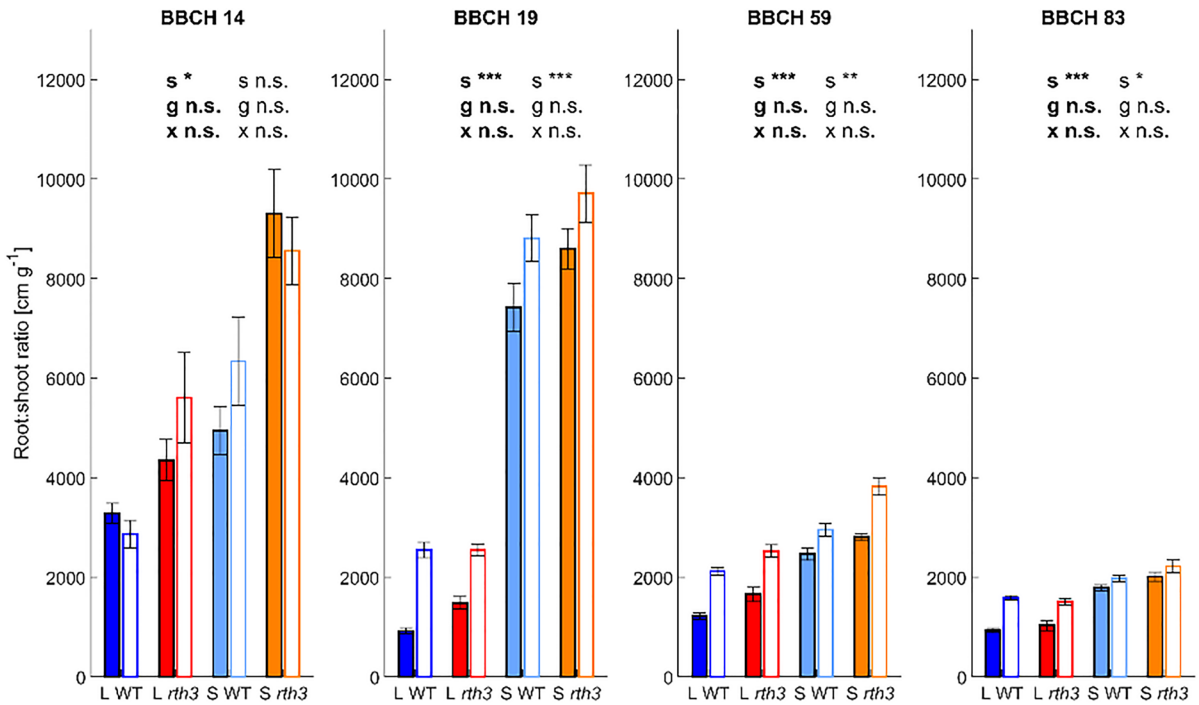
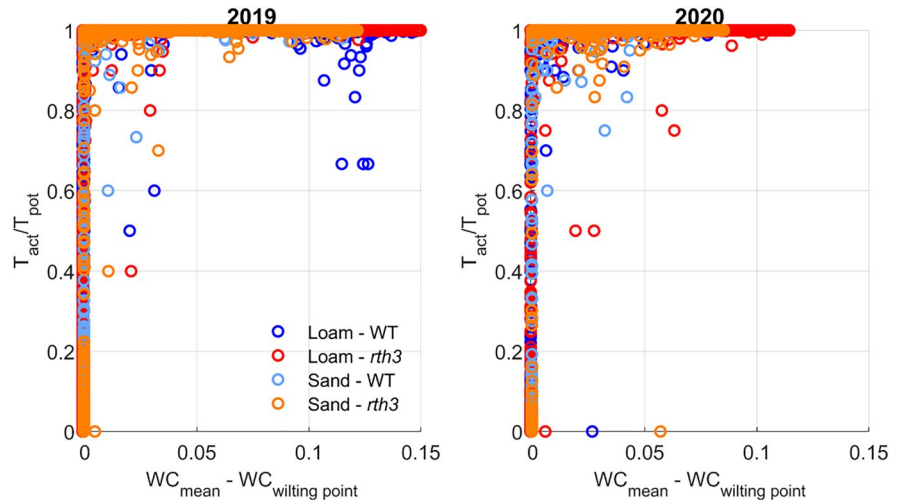


Fig. 11 Impact of substrate (loam – L, sand - S) and maize genotype (wild-type—WT, root hair mutant *rth3*–*rth3*) on the root-shoot ratio (cm root per g of dry shoot biomass) at different stages of plant development (BBCH 14, BBCH 19, BBCH 59 and BBCH 83) in the first (2019 – colored bars) and second

(2020 – white bars) year. A 2-factorial ANOVA and posthoc Tukey’s test was performed per each development stage and year. Significant effect of factor is indicated by s for substrate, g for genotype and x for interaction; bold letters refer to 2019

Fig. 12 Simulated stress defined as the ration of actual to potential transpiration (T_{act}/T_{pot}) versus the plant available water content in the soil



Discussion

We discuss first the observed and simulated root water uptake and water losses and the amount of

water that could be extracted by the root systems, which was surprisingly similar for the different substrates and similar for the two genotypes with and without root hairs. We relate this finding to

Fig. 13 Simulated midday water sink for 4 soil layers (0–20, 20–40, 40–60 and 60–75 cm) for the loam wild-type treatment

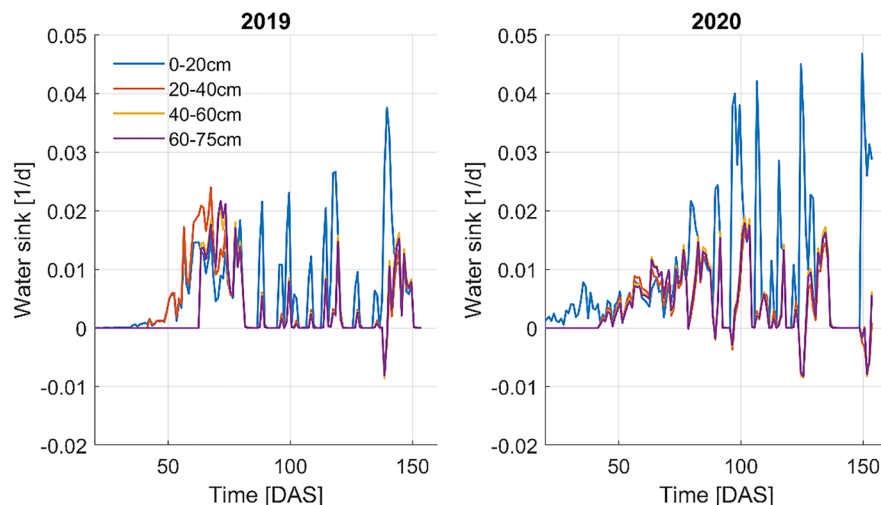
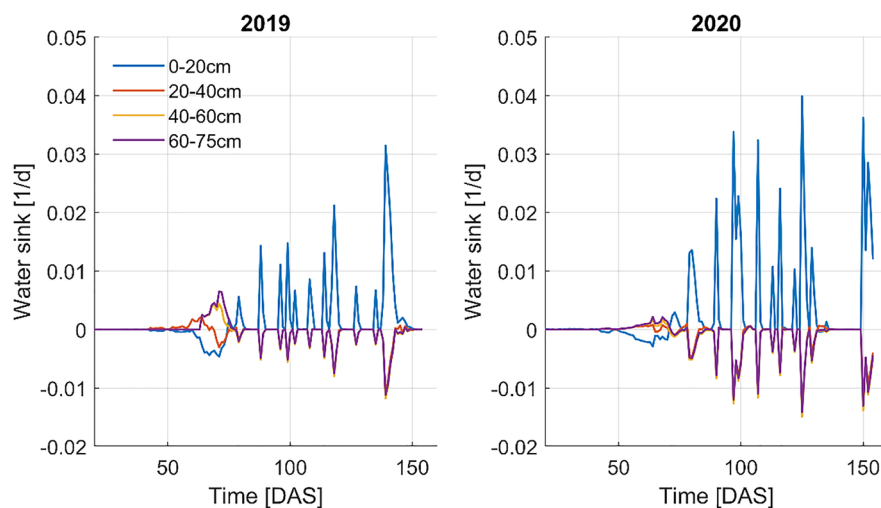


Fig. 14 Simulated mid-night water sink for 4 soil layers (0–20, 20–40, 40–60 and 60–75 cm) for the loam wild-type treatment



root and shoot properties and how they changed during the growing seasons in the two different substrates. In a second part, we discuss the differences between simulated and observed leaf water potentials and speculate how these differences are associated with rhizosphere processes and influenced by root hairs. In the third part, we discuss how the observed water uptake processes could have been impacted by nutrient deficiency in the substrates. Finally, we compare the results of our field study in maize with a similar field study in barley.

The measured total water extraction from the soil showed that the accuracy of our soil moisture measurements was too low to observe differences between

treatments. Despite a high precision, i.e. a low standard error of the mean, of our soil moisture measurements, the placement of water content sensors in preferential flow pathways might have led to artifacts in the estimation of water losses from the soil. The effect of maize rows on lateral variations in water content has been documented in several studies (Beff et al. 2013; Hupet and Vanclooster 2005; Michot et al. 2003) and might explain why the accuracy of the soil moisture measurements to represent mean soil moisture content in the plot was lower than the precision.

Due to the high root system conductance, which was estimated from the root density, the root systems in the simulation model were very effective in extracting all water in the soil profile that was accessible to

plants. A root system conductance in the order of 10^{-3} d^{-1} (Fig. 3) and a critical leaf water potential of -1.6 MPa or $-1.6 \cdot 10^2 \text{ m}$ hydraulic head implies that a transpiration rate of 16 mm d^{-1} (corresponding with a maximal rate at midday when the average daily transpiration is 4 mm d^{-1}) can be sustained when only 10% of the total root length is within wet soil (with hydraulic head close to 0 m) and taking up water whereas the other fraction of the total root length is in dry soil (where soil water hydraulic head is equal to $-1.6 \cdot 10^2 \text{ m}$). According to the simulations, the crop could redistribute the water uptake within the root zone so that the distribution of both water and roots in the root zone hardly affected the total root water uptake and uptake was not limited until the average water content in the root zone reached a critical value. These results are consistent with a study by Guswa et al. (2002) who showed that when the fraction of roots in wet soil required to take up the transpiration demand is small (10%), the water distribution in the root zone hardly affects the root water uptake.

The simulated redistribution of root water uptake towards deeper soil layers during the first phase of the growing season, when there was still water present in these layer, was facilitated by the high root densities deeper in the soil profile, which could be interpreted as an adaptation of the root system to the dry soil conditions (Amos and Walters 2006; Kondo et al. 2000). Our measured root-shoot ratios are quite large when compared with other maize data, which is another indication of the adaptation of the root system. Root and shoot data gathered from different locations in the Midwest (US) by Ordonez et al. (2020) show a mean root-shoot ratio of 880 cm/g during the grain filling stage, which should correspond to our data at BBCH59 (98 DAS). In addition, our measured RLD data in loam is generally larger than that reported in other studies about maize (Gao et al. 2010; Morandage et al. 2021). The root length normalized root system conductance used in the simulation, $8.64 \cdot 10^{-6} \text{ cm d}^{-1}$, was within the lower range of conductances reported for several crops by Belmans et al. (1979) (10^{-13} to $10^{-10} \text{ m s}^{-1}$ or $8.64 \cdot 10^{-7}$ to $8.64 \cdot 10^{-4} \text{ cm d}^{-1}$) and similar to the value reported by Cai et al. (2018b) for winter wheat, $2.5 \cdot 10^{-6} \text{ cm d}^{-1}$. The high root system conductances used in our simulations, i.e. in the order of 10^{-3} d^{-1} , which were in the higher range of root system conductivities for Maize calculated by Meunier et al. (2019) (ranging between 10^{-9}

and $10^{-7} \text{ m}^3 \text{ MPa}^{-1} \text{ s}^{-1} \text{ plant}^{-1}$ corresponding with a range between $8.64 \cdot 10^{-6}$ and $8.64 \cdot 10^{-3} \text{ d}^{-1}$ for 10 plants m^{-2}) are therefore attributed to the high root densities of the maize crop in all treatments. The high root system conductance despite the relatively low root length normalized conductance is also in agreement with the sensitivity analysis performed by Meunier et al. (2019) showing that more than 2/3 of the variability of root system conductances of maize plants could be attributed to variability in root architecture, which includes root length, whereas only 1/4 of the variability was attributed to root segment hydraulic properties. However, the analysis of Meunier et al. (2019) neither included the impact of root hairs nor the impact of rhizosphere conductivity and only focused on the root system hydraulic conductance.

The high root system conductance assumed in the simulations resulted in low sensitivity of the simulated cumulative transpiration and soil water balance to stomatal regulation of transpiration, i.e. the presumed relation between stomatal conductance and leaf water potential. In our simulation, this relation was a very simple relation that corresponds with a step function of stomatal conductance versus leaf water potential. Using a more negative threshold of the critical leaf water potential did not influence the simulated cumulative transpiration considerably. Based on the water retention curves (Fig. S1), we anticipate that a less negative threshold, e.g., -1 MPa instead of -1.6 MPa would not have a big impact on the simulated cumulative transpiration either. However, the abrupt stomatal regulation that we considered in our model, i.e., no regulation until a threshold leaf water potential is reached and a perfectly isohydric behavior when this threshold is reached, in combination with the high root system conductance led to an abrupt decrease in simulated transpiration when the threshold leaf water potential was reached. Such a drastic cease in transpiration predicted by the model during stress periods was not observed in the sap flow measurements (Fig. 6). This might indicate that the studied maize genotypes started closing stomata already at less negative leaf water potentials saving soil water and avoided a complete closure of stomata and strong reduction in transpiration at more negative leaf water potentials. However, the effect of this more gradual regulation of stomatal opening as a function of leaf water potential was hardly noticeable in the soil water balance.

In all treatments, the simulated evaporation of water from the soil surface at the beginning of the growing season when the crop did not fully cover the soil surface was a considerable fraction of the total amount of water lost during the growing season by evapotranspiration ranging between roughly 30% and 50% of the total amount of water lost. The contribution of evaporation to the total evapotranspiration losses in maize can vary considerably depending on climate and irrigation practices (e.g. sprinkling irrigation) and Kool et al. (2014) report values of measured evaporation to evapotranspiration ratios for maize between 0 and 0.78. Consequently, when this evaporative water loss was considered, the WUE of the field plots was drastically reduced compared to the WUE of the individual plants. The evaporative losses were larger in the loam as compared to the sand, which is a consequence of the higher unsaturated hydraulic conductivity of the loam so that water can be transported by capillary flow over a larger distance from the wetter subsoil to the evaporating soil surface than in the sand. Simulated evaporative losses were also larger for the mutant *rth3* than for the WT which is a consequence of the lower LAI of the mutant so that more radiation reaches the soil surface and can be used to evaporate water. The approach that we used to model evaporation from the soil surface as a function of LAI is very crude and does not account for the aerodynamic transfer resistance in the canopy. In order to simulate how much water lost from the plot is actually used or transpired by the plant, it is important to estimate the crop cover or LAI.

In our study, we did not simulate LAI or crop cover but derived it from observations. Especially for maize, leaf elongation depends strongly on leaf water potential and lower leaf water potentials may impact leaf development before they have an impact on stomatal closure (Chenu et al. 2008). This is consistent with concepts used in crop models such as Aquacrop (Hsiao et al. 2009; Raes et al. 2009; Steduto et al. 2009) that consider an impact of water stress on leaf elongation and canopy development that sets on for less dry soil conditions than stomatal closure. It should be noted that Aquacrop does not consider the link between soil water content, plant water status and plant hydraulics. The impact of root hairs on crop transpiration and water use might be via the effect on leaf water potential before stomatal closure occurs and the consequent effects on plant growth. Before

simulated stomatal closure (i.e., before the transpiration rate was reduced compared to the potential transpiration rate), the measured leaf water potentials deviated more from the simulated leaf water potentials for the *rth3* mutant than for the WT in both soil types (Fig. 8). This indicates that, after putting the measured leaf water potentials in context of the different crop development of the two genotypes, the *rth3* mutant showed lower leaf water potentials than the WT. We speculate that these lower leaf water potentials associated with a lack of root hairs were caused by a poorer soil-root contact and a larger contact resistance at intermediate soil moisture contents. This might be one reason for the slower development and lower LAI of the *rth3* mutant than the WT. A more accurate simulation of the leaf water potentials during the early stages of the crop development considering rhizosphere processes and the impact of root hairs on plant water potentials would in this respect be important to improve the prediction of LAI and crop development before water stress leads to stomatal closure and reduces potential transpiration. The high root system conductances for both the wild type and root hairless mutant made that stomatal closure was simulated only when the soil was dry, the soil conductivity became limiting, and the impact of the enhanced soil-root contact by the root hairs was lost (the contact may be lost also due to root hair shrinkage (Duddek et al. 2022)) so that the wild type and the hairless mutant reduced transpiration at similar soil water contents.

The comparison between simulated and measured leaf water potentials in 2020 indicated that the model overestimated leaf water potentials (simulated values were less negative) for all treatments. One reason could be that we overestimated the root conductance since a substantial share of aerenchyma was observed in the cortex of the main root axis already at BBCH 19 (Vetterlein et al. 2022). Another reason could be the soil-root conductance, which was not included in the model. This is supported by results reported by Cai et al. (2022) who compiled data from several lab experiments and found that, especially in sandy soils, a low soil-root conductance generates a drop in soil water potentials from the bulk soil to the soil-root interface and leads to a strong decrease in leaf water potentials (Abdalla et al. 2021). The drop in soil water potential depends on the unsaturated hydraulic conductivity of the rhizosphere, which decreases strongly

when the soil dries out. Since the unsaturated hydraulic conductivity decreases much more with decreasing soil water potential in sand than in loam, the drop in water potential between the bulk soil and the root surface for a given water flux to the root surface is considerably larger and emerges at higher bulk soil water potentials in sand than in loam (Cai et al. 2021). Local drops in the soil water potential around roots can lead to a more negative soil water potential felt by the plant than the bulk soil water potentials, and thus more negative leaf water potentials as compared to simulated ones (which did not consider this drop in water potential between the bulk soil and the soil-root interface). This drop in water potential increases with the water flux to the root surfaces. Higher root length density and larger root radii in the sand than in the loam reduce these local fluxes and mitigate the potential drops that are caused by the reduced soil hydraulic conductivities in the sand. Therefore, the impact of soil hydraulic properties on plant water status and leaf water potentials should be assessed considering also the root system properties and architecture.

Including the rhizosphere in the model therefore seems to be important to improve the predictions of the leaf water potentials and the plant water status and how they depend on soil and root system properties. This would allow one to account also for modifications of the rhizosphere properties that are induced by roots, e.g. compaction and loosening of the soil around roots and the impact of root exudates on rhizosphere properties (Landl et al. 2021) and to account for the effect of root hairs on soil-root contacts and the mitigation of water potential drops in the rhizosphere. Efficient numerical approaches have been implemented in 3D root architecture models to simulate the impact of rhizosphere processes on water and nutrient uptake (Khare et al. 2022; Mai et al. 2019; Schröder et al. 2009) showing that including rhizosphere processes in simulation models leads to lower predictions of water and nutrient uptake. The model that was used in this paper and that is based on the approach introduced by Couvreur et al. (2014) is an upscaled 1D version of the detailed 3D root models and therefore considers root hydraulics and reproduces processes like root water uptake compensation, redistribution and hydraulic lift. But it does not consider rhizosphere processes and we are currently testing and developing approaches to upscale coupled rhizosphere and root hydraulic models to 1D

simulation models. Despite not considering rhizosphere processes, the model predicted the onset of water stress, here defined as the time when the transpiration rate was reduced, quite accurately. These simulation model comparisons as well as lab experiments investigating the role of rhizosphere processes considered non-growing root systems, a single drying cycle, and a uniform initial soil moisture distribution. Root system development with roots growing into wetter regions of the soil, water redistribution by root systems after rainfall events, and water uptake redistribution as a consequence of root hydraulics when the soil water is not uniformly distributed in the root zone might therefore mask the impact of local rhizosphere processes on the crop stand water balance. Whether this masking also implies an overruling of local rhizosphere processes still requires further investigation. A water isotope labeling study showed that the redistribution of water and hydraulic lift via the root system were overestimated when the rhizosphere conductance or resistance was not included in the model (Meunier et al. 2018a). But again, the importance of these rhizosphere processes and the role of root hairs in it for the soil water balance remains to be investigated further.

An equally important factor as the water stress, which influences the development of the two genotypes in the two different soils, is nutrient stress since all treatments were sub-optimally fertilized. Our large root-shoot ratios and root length density data might indicate a response of the plant to nutrient deficiency. Early P and K deficiencies which increased with time more in sand compared to loam might have driven larger investment into root growth in sand. This was accelerated by the general stronger dependency on surface applied fertilizer in sand due to the lower initial nutrient content of sand which could explain the higher root density near the soil surface in the sand versus the more uniform root density distribution in the sand (detailed discussion in Vetterlein et al. (2022)). It is likely that both factors (P starvation and lack of irrigation) led to large root-shoot ratios in our study, thus leading to a very efficient root system in taking up water compared to canopy demands. This is supported by a study by Mollier and Pellerin (1999) showing that phosphorus starvation as well as a lower number of irrigation events led larger root-shoot ratios as compared to control treatments. Furthermore, larger root-shoot ratios in the *rth3* genotype

compared to the WT might also suggest a response of the plant to compensate for the lack of root hairs and was consistent with lab scale experiments of the same treatments (Lippold et al. 2021). Nutrient deficiencies might also trigger aquaporin (water transporters in cell membranes) gene expression and activation, which increase the radial conductance of root segments and improve water uptake. During the field experiments, aquaporin gene expression was monitored over the growing season and in the different treatments (ongoing work). Gene expression was primarily affected by plant development, with some minor differences between substrates. Aquaporin gene expression was higher in sand compared to loam substrate but root hair formation did not significantly affect aquaporin gene expression patterns. Because of the high root system conductance due to the high root length density, the root distribution in the soil profile does not have an important impact on the total water uptake from the root zone (in the same way as the water distribution does not have a large impact). Since the sensitivity of root water uptake and crop growth to the root system conductance becomes small when the conductance becomes large (Nguyen et al. 2022; Nguyen et al. 2020), the effect of differences in aquaporin activity between the different treatments and within the root zone is hard to disentangle. Therefore, we do not expect that more root development in the top layer of the sandy soil and larger aquaporin gene expression in the sand had an important additional impact on total water uptake. Whether removal of water stress by irrigation or more rainfall will result in better crop development when nutrient stress is not alleviated by extra fertilization remains to be further investigated. A two factorial experimental study with rice grown under different combinations of P and water deficiency showed that under deficient P supply, irrigation did not increase P uptake and growth whereas under optimal P supply, irrigation had an effect on P uptake and growth (De Bauw et al. 2020). The prediction of root water and P uptake in that study depended strongly on the root system that differed considerably among the different treatments.

When comparing our results with those of Marin et al. (2021), who carried out a two-year field experiment, one year with normal precipitation without drought stress and one year with very low precipitation with drought stress, in two soils: a sandy loam and a clay loam, with different barley genotypes

including genotypes without root hairs, we found similarities but also a few differences. In both studies, a longer total root length was observed in the coarser soil. The shoot biomass of barley (Marin et al. 2021) was larger in the coarser soil whereas no difference in final biomass of maize between the two soils was observed in our study. The shoot biomass of the hairless mutant was generally lower than that of the WT in both studies. During the dry year, lower leaf water potentials of barley were observed in the coarser soil than in the finer soil and the hairless barley mutant had lower leaf water potentials than the WT in the finer soil. In our study, the direct comparison of maize leaf water potentials between genotypes and soil types required a more careful interpretation since the crop development and the evolution of the transpiration differed considerably between the different treatments. Maize development and transpiration increased faster in the finer soil and for the WT so that these two factors resulted in an earlier emergence of stress. Comparing leaf water potentials in the different treatments at the same time reflects the crop status at that time but not whether a certain combination of factors reduced or increased water stress.

Conclusions

One of our starting hypotheses was that root hairs influence root water uptake and that a genotype lacking root hairs would reduce transpiration at less negative soil water potentials than the WT, especially in sand. This hypothesis would correspond with an earlier reduction in transpiration by the hairless mutant than the wild type and, since the plant available water that was stored at the time of sowing was similar in sand and loam, earlier in the sand than in the loam. The opposite was observed. Based on simulations, the earlier reduction of water uptake in the loam than in the sand for both genotypes could be attributed to a faster shoot and leaf area development and hence a larger water consumption in the loam. However, the total water use over the whole growing season, simulated and observed, was similar in both soil types and genotypes. Simulations of root water uptake that were based on observed root length densities and root length normalized root conductance derived from literature data, showed that the root systems of the WT and the hairless *rth3*

mutant could extract almost all plant available water in both the sand and loam, which was confirmed by the observed soil water depletion. Therefore, we could not confirm our hypothesis that root hairs influence root water uptake. These findings are in line with recent lab experiments using the same soil types and genotypes (Cai et al. 2021).

A second hypothesis was that plants adapt their root system to the environmental conditions and that a root hairless genotype could compensate a presumed reduction in root water uptake by growing more roots. We found that both genotypes grew more roots in the sand than in the loam supporting this hypothesis, but the hairless *rth3* mutant grew less roots than the WT, which does not confirm our hypothesis. For all treatments, simulations suggested that root systems were ‘oversized’ for water acquisition since the water demand by the shoot could be extracted when only 10% of the total root length was in wet soil and active in root water uptake. Therefore, the root system could redistribute the uptake to wetter zones in the root zone and compensate for a lower uptake from drier soil layers. This enables the root system to effectively extract water from a soil profile with a non-uniform water distribution, i.e., with more water in the subsoil at the start of the growing season and higher water contents near the soil surface by incoming rain or irrigation later in the growing season. The model also simulated a considerable amount of water that was redistributed via the root system from wetter to drier soil layers bypassing the soil pore volume. The role of this water redistribution within the soil profile for the water availability to the crop needs to be investigated further.

The shoot growth differed between the two genotypes with larger shoots for the WT. This difference between genotypes could point at the role of root hairs in nutrient uptake and growth since nutrient concentrations, especially P, were suboptimal in both soils, as was also evidenced by the observation of purple discoloration of leaves. Another explanation could be the lower leaf water potentials in the *rth3* genotype than in the WT, which might affect leaf expansion and growth. The model simulations, which did not consider rhizosphere processes and the potential role of root hairs in improving the soil-root contact and reducing water potential gradients between the bulk soil and the root surface,

overestimated the leaf water potential and more so in the hairless *rth3* mutant and in the sandy soil. Including these rhizosphere processes and how they are influenced by root hairs in the simulation model may therefore be important to predict plant water status at intermediate soil wetness and less negative leaf water potentials before onset of water stress (i.e., reduction in transpiration) better and, linked to it, plant growth. Under these conditions, soil-root contact is influenced by root hairs whereas it breaks under dry conditions. The extent to which the root systems could dry out both soils before transpiration was reduced, depended less on this soil-root contact and could be simulated based on root density, root distribution, root conductance, and root growth.

Acknowledgements For supporting the maintenance of the field experiment and the sampling events we would like to thank Sebastian Häusler, Eric Braatz, Susanne Schreiter, Anke Coolens and Asegidew Akale Zebene. Without their care and patience this study would not have been possible. We would like to acknowledge the support from Bad Lauchstädt field station (Ines Merbach, Konrad Kirsch, Sven Meyer, Sabine Straßenburg, Steffi Wagner, Thomas Bienert, Birgit Sawall). Seeds of the maize mutant *rth3* were provided by Caroline Macron and Frank Hochholdinger (University Bonn). We would like to thank the reviewers for their helpful comments and suggestions.

Funding Open Access funding enabled and organized by Projekt DEAL. This project was carried out in the framework of the project “Emerging effects of root hairs and mucilage on plant scale soil water relations” of the priority program 2089 “Rhizosphere spatiotemporal organization - a key to rhizosphere functions” funded by DFG, German Research Foundation (project numbers: 403801423, 403670197).

Open Access This article is licensed under a Creative Commons Attribution 4.0 International License, which permits use, sharing, adaptation, distribution and reproduction in any medium or format, as long as you give appropriate credit to the original author(s) and the source, provide a link to the Creative Commons licence, and indicate if changes were made. The images or other third party material in this article are included in the article’s Creative Commons licence, unless indicated otherwise in a credit line to the material. If material is not included in the article’s Creative Commons licence and your intended use is not permitted by statutory regulation or exceeds the permitted use, you will need to obtain permission directly from the copyright holder. To view a copy of this licence, visit <http://creativecommons.org/licenses/by/4.0/>.

References

- Abdalla M, Carminati A, Cai GC, Javaux M, Ahmed MA (2021) Stomatal closure of tomato under drought is driven by an increase in soil-root hydraulic resistance. *Plant Cell Environ* 44:425–431. <https://doi.org/10.1111/pce.13939>
- Allen RG, Pereira LS, Raes D, Smith M (1998) Crop evapotranspiration: guidelines for computing crop water requirements. FAO, Rome
- Amos B, Walters DT (2006) Maize root biomass and net rhizodeposited carbon: an analysis of the literature. *Soil Sci Soc Am J* 70:1489–1503. <https://doi.org/10.2136/sssaj2005.0216>
- Awal MA, Koshi H, Ikeda T (2006) Radiation interception and use by maize/peanut intercrop canopy. *Agric For Meteorol* 139:74–83. <https://doi.org/10.1016/j.agrformet.2006.06.001>
- Baret F, Madec S, Irfan K, Lopez J, Comar A, Hemmerle M, Dutartre D, Praud S, Tixier MH (2018) Leaf-rolling in maize crops: from leaf scoring to canopy-level measurements for phenotyping. *J Exp Bot* 69:2705–2716. <https://doi.org/10.1093/jxb/ery071>
- Beff L, Gunther T, Vandoorne B, Couvreur V, Javaux M (2013) Three-dimensional monitoring of soil water content in a maize field using electrical resistivity tomography. *Hydrol Earth Syst Sci* 17:595–609. <https://doi.org/10.5194/hess-17-595-2013>
- Belmans C, Feyen J, Hillel D (1979) Attempt at experimental validation of macroscopic-scale models of soil-moisture extraction by roots. *Soil Sci* 127:174–186. <https://doi.org/10.1097/00010694-197903000-00007>
- Cai GC, Vanderborght J, Couvreur V, Mboh CM, Vereecken H (2018a) Parameterization of root water uptake models considering dynamic root distributions and water uptake compensation. *Vadose Zone J* 17. <https://doi.org/10.2136/vzj2016.12.0125>
- Cai GC, Vanderborght J, Langensiepen M, Schnepf A, Hugging H, Vereecken H (2018b) Root growth, water uptake, and sap flow of winter wheat in response to different soil water conditions. *Hydrol Earth Syst Sci* 22:2449–2470. <https://doi.org/10.5194/hess-22-2449-2018>
- Cai GC, Carminati A, Abdalla M, Ahmed MA (2021) Soil textures rather than root hairs dominate water uptake and soil-plant hydraulics under drought. *Plant Physiol* 187:858–872. <https://doi.org/10.1093/plphys/kiab271>
- Cai GC, Ahmed MA, Abdalla M, Carminati A (2022) Root hydraulic phenotypes impacting water uptake in drying soils. *Plant Cell Environ* 45:650–663. <https://doi.org/10.1111/pce.14259>
- Carminati A, Passioura JB, Zarebanadkouki M, Ahmed MA, Ryan PR, Watt M, Delhaize E (2017) Root hairs enable high transpiration rates in drying soils. *New Phytol* 216:771–781. <https://doi.org/10.1111/nph.14715>
- Chenu K, Chapman SC, Hammer GL, McLean G, Salah HBH, Tardieu F (2008) Short-term responses of leaf growth rate to water deficit scale up to whole-plant and crop levels: an integrated modelling approach in maize. *Plant Cell Environ* 31:378–391. <https://doi.org/10.1111/j.1365-3040.2007.01772.x>
- Couvreur V, Vanderborght J, Javaux M (2012) A simple three-dimensional macroscopic root water uptake model based on the hydraulic architecture approach. *Hydrol Earth Syst Sci* 16:2957–2971. <https://doi.org/10.5194/hess-16-2957-2012>
- Couvreur V, Vanderborght J, Beff L, Javaux M (2014) Horizontal soil water potential heterogeneity: simplifying approaches for crop water dynamics models. *Hydrol Earth Syst Sci* 18:1723–1743. <https://doi.org/10.5194/hess-18-1723-2014>
- De Bauw P, Mai TH, Schnepf A, Merckx R, Smolders E, Vanderborght J (2020) A functional-structural model of upland rice root systems reveals the importance of laterals and growing root tips for phosphate uptake from wet and dry soils. *Ann Bot* 126:789–806. <https://doi.org/10.1093/aob/mcaa120>
- Dodd IC, Diatloff E (2016) Enhanced root growth of the brb (bald root barley) mutant in drying soil allows similar shoot physiological responses to soil water deficit as wild-type plants. *Funct Plant Biol* 43:199–206. <https://doi.org/10.1071/fp15303>
- Duddek P, Carminati A, Koebernick N, Ohmann L, Lovric G, Delzon S, Rodriguez-Dominguez CM, King A, Ahmed MA (2022) The impact of drought-induced root and root hair shrinkage on root-soil contact. *Plant Physiol*. <https://doi.org/10.1093/plphys/kiac144>
- Durner W (1994) Hydraulic conductivity estimation for soils with heterogeneous pore structure. *Water Resour Res* 30:211–223. <https://doi.org/10.1029/93wr02676>
- Flenet F, Kiniry JR, Board JE, Westgate ME, Reicosky DC (1996) Row spacing effects on light extinction coefficients of corn, sorghum, soybean, and sunflower. *Agron J* 88:185–190. <https://doi.org/10.2134/agronj1996.00021962008800020011x>
- Gao Y, Duan AW, Qiu XQ, Liu ZG, Sun JS, Zhang JP, Wang HZ (2010) Distribution of roots and root length density in a maize/soybean strip intercropping system. *Agric Water Manag* 98:199–212. <https://doi.org/10.1016/j.agwat.2010.08.021>
- Guswa AJ, Celia MA, Rodriguez-Iturbe I (2002) Models of soil moisture dynamics in ecohydrology: a comparative study. *Water Resour Res* 38: 5–1–5–15. <https://doi.org/10.1029/2001WR000826>
- Hendrickx JMH, Flury M (2001) Uniform and preferential flow mechanisms in the vadose zone. Workshop on Conceptual Models of Flow and Transport in the Fractured Vadose Zone, Washington, D.C.
- Hochholdinger F, Wen TJ, Zimmermann R, Chimot-Marolle P, Silva ODE, Bruce W, Lamkey KR, Wienand U, Schnable PS (2008) The maize (*Zea mays* L.) roothairless3 gene encodes a putative GPI-anchored, monocot-specific, COBRA-like protein that significantly affects grain yield. *Plant J* 54:888–898. <https://doi.org/10.1111/j.1365-313X.2008.03459.x>
- Hsiao TC, Heng L, Steduto P, Rojas-Lara B, Raes D, Fereres E (2009) AquaCrop—the FAO crop model to simulate yield response to water: III. Parameterization and testing for maize. *Agron J* 101:448–459. <https://doi.org/10.2134/agronj2008.0218s>
- Hupet F, Vanclooster A (2005) Micro-variability of hydrological processes at the maize row scale: implications for soil

- water content measurements and evapotranspiration estimates. *J Hydrol* 303:247–270. <https://doi.org/10.1016/j.jhydrol.2004.07.017>
- Kadioglu A, Terzi R, Saruhan N, Saglam A (2012) Current advances in the investigation of leaf rolling caused by biotic and abiotic stress factors. *Plant Sci* 182:42–48. <https://doi.org/10.1016/j.plantsci.2011.01.013>
- Khare D, Selzner T, Leitner D, Vanderborght J, Vereecken H, Schnepf A (2022) Root system scale models significantly overestimate root water uptake at drying soil conditions. *Front Plant Sci* 13. <https://doi.org/10.3389/fpls.2022.798741>
- Kondo M, Murty MVR, Aragonés DV (2000) Characteristics of root growth and water uptake from soil in upland rice and maize under water stress. *Soil Science and Plant Nutrition* 46:721–732. <https://doi.org/10.1080/00380768.2000.10409137>
- Kool D, Agam N, Lazarovitch N, Heitman JL, Sauer TJ, Bengali A (2014) A review of approaches for evapotranspiration partitioning. *Agric For Meteorol* 184:56–70. <https://doi.org/10.1016/j.agrformet.2013.09.003>
- Lancashire PD, Bleiholder H, Vandenboom T, Langeluddeke P, Stauss R, Weber E, Witzemberger A (1991) A uniform decimal code for growth-stages of crops and weeds. *Ann Appl Biol* 119:561–601. <https://doi.org/10.1111/j.1744-7348.1991.tb04895.x>
- Landl M, Phalempin M, Schlüter S, Vetterlein D, Vanderborght J, Kroener E, Schnepf A (2021) Modeling the impact of rhizosphere bulk density and mucilage gradients on root water uptake. *Frontiers in Agronomy* 3. <https://doi.org/10.3389/fagro.2021.622367>
- Leitner D, Meunier F, Bodner G, Javaux M, Schnepf A (2014) Impact of contrasted maize root traits at flowering on water stress tolerance - a simulation study. *Field Crop Res* 165:125–137. <https://doi.org/10.1016/j.fcr.2014.05.009>
- Lippold E, Phalempin M, Schlüter S, Vetterlein D (2021) Does the lack of root hairs alter root system architecture of *Zea mays*? *Plant Soil* 467:267–286. <https://doi.org/10.1007/s11104-021-05084-8>
- Lynch JP (2013) Steep, cheap and deep: an ideotype to optimize water and N acquisition by maize root systems. *Ann Bot* 112:347–357. <https://doi.org/10.1093/aob/mcs293>
- Mai TH, Schnepf A, Vereecken H, Vanderborght J (2019) Continuum multiscale model of root water and nutrient uptake from soil with explicit consideration of the 3D root architecture and the rhizosphere gradients. *Plant Soil* 439:273–292. <https://doi.org/10.1007/s11104-018-3890-4>
- Marin M, Feeney DS, Brown LK, Naveed M, Ruiz S, Koebernick N, Bengough AG, Hallett PD, Roose T, Puertolas J, Dodd IC, George TS (2021) Significance of root hairs for plant performance under contrasting field conditions and water deficit. *Ann Bot* 128:1–16. <https://doi.org/10.1093/aob/mcaa181>
- Meunier F, Rothfuss Y, Bariac T, Biron P, Richard P, Durand JL, Couvreur V, Vanderborght J, Javaux M (2018a) Measuring and modeling hydraulic lift of *Lolium multiflorum* using stable water isotopes. *Vadose Zone J* 17. <https://doi.org/10.2136/vzj2016.12.0134>
- Meunier F, Zarebanadkouki M, Ahmed MA, Carminati A, Couvreur V, Javaux M (2018b) Hydraulic conductivity of soil-growth lupine and maize unbranched roots and maize root-shoot junctions. *J Plant Physiol* 227:31–44. <https://doi.org/10.1016/j.jplph.2017.12.019>
- Meunier F, Heymans A, Draye X, Couvreur V, Javaux M, Lobet G (2019) MARSHAL, a novel tool for virtual phenotyping of maize root system hydraulic architectures. *In silico Plants* 2. <https://doi.org/10.1093/inilicoplants/diz012>
- Meyer N, Welp G, Amelung W (2018) The temperature sensitivity (Q10) of soil respiration: controlling factors and spatial prediction at regional scale based on environmental soil classes. *Glob Biogeochem Cycle* 32:306–323. <https://doi.org/10.1002/2017gb005644>
- Michot D, Benderitter Y, Dorigny A, Nicoulaud B, King D, Tabbagh A (2003) Spatial and temporal monitoring of soil water content with an irrigated corn crop cover using surface electrical resistivity tomography. *Water Resour Res* 39:1138. <https://doi.org/10.1029/2002WR001581>
- Mokhtarpour H, Teh CB, Saleh G, Selamat AB, Asadi ME, Kamkar B (2010) Non-destructive estimation of maize leaf area, fresh weight, and dry weight using leaf length and leaf width. *Communications in Biometry and Crop Science* 5:19–26
- Mollier A, Pellerin S (1999) Maize root system growth and development as influenced by phosphorus deficiency. *J Exp Bot* 50:487–497. <https://doi.org/10.1093/jexbot/50.333.487>
- Morandage S, Vanderborght J, Zorner M, Cai GC, Leitner D, Vereecken H, Schnepf A (2021) Root architecture development in stony soils. *Vadose Zone J* 20. <https://doi.org/10.1002/vzj2.20133>
- Nguyen TH, Langensiepen M, Vanderborght J, Hüging H, Mboh CM, Ewert F (2020) Comparison of root water uptake models in simulating CO₂ and H₂O fluxes and growth of wheat. *Hydrol Earth Syst Sci* 24:4943–4969. <https://doi.org/10.5194/hess-24-4943-2020>
- Nguyen TH, Langensiepen M, Hueging H, Gaiser T, Seidel SJ, Ewert F (2022) Expansion and evaluation of two coupled root–shoot models in simulating CO₂ and H₂O fluxes and growth of maize. *Vadose Zone J* n/a: e20181. <https://doi.org/10.1002/vzj2.20181>
- Novick KA, Ficklin DL, Baldocchi D, Davis KJ, Ghezzehei TA, Konings AG, MacBean N, Raouf N, Scott RL, Shi Y, Sulman BN, Wood JD (2022) Confronting the water potential information gap. *Nat Geosci* 15:158–164. <https://doi.org/10.1038/s41561-022-00909-2>
- Ordonez RA, Archontoulis SV, Martinez-Feria R, Hatfield JL, Wright EE, Castellano MJ (2020) Root to shoot and carbon to nitrogen ratios of maize and soybean crops in the US Midwest. *Eur J Agron* 120. <https://doi.org/10.1016/j.eja.2020.126130>
- Poorter H, Bühler J, van Dusschoten D, Climent J, Postma JA (2012) Pot size matters: a meta-analysis of the effects of rooting volume on plant growth. *Funct Plant Biol* 39:839–850. <https://doi.org/10.1071/FP12049>
- Raes D, Steduto P, Hsiao TC, Fereres E (2009) AquaCrop—the FAO crop model to simulate yield response to water: II. Main algorithms and software description. *Agron J* 101:438–447. <https://doi.org/10.2134/agronj2008.0140s>
- Ritchie JT (1972) Model for predicting evaporation from a row crop with incomplete cover. *Water Resour Res* 8:1204. <https://doi.org/10.1029/WR008i005p01204>
- Schröder T, Javaux M, Vanderborght J, Körffgen B, Vereecken H (2009) Implementation of a microscopic soil-root

- hydraulic conductivity drop function in a three-dimensional soil-root architecture water transfer model. *Vadose Zone J* 8:783–792. <https://doi.org/10.2136/vzj2008.0116>
- Segal E, Kushnir T, Mualem Y, Shani U (2008) Water uptake and hydraulics of the root hair rhizosphere. *Vadose Zone J* 7:1027–1034. <https://doi.org/10.2136/vzj2007.0122>
- Šimůnek J, van Genuchten MT, Šejna M (2016) Recent developments and applications of the HYDRUS computer software packages. *Vadose Zone J* 15. <https://doi.org/10.2136/vzj2016.04.0033>
- Steduto P, Hsiao TC, Raes D, Fereres E (2009) AquaCrop—the FAO crop model to simulate yield response to water: I. concepts and underlying principles. *Agron J* 101:426–437. <https://doi.org/10.2134/agronj2008.0139s>
- Suzuki N, Taketa S, Ichii M (2003) Morphological and physiological characteristics of a root-hairless mutant in rice (*Oryza sativa* L.). *Plant Soil* 255:9–17. <https://doi.org/10.1023/a:1026180318923>
- Tron S, Bodner G, Laio F, Ridolfi L, Leitner D (2015) Can diversity in root architecture explain plant water use efficiency? A modeling study. *Ecol Model* 312:200–210. <https://doi.org/10.1016/j.ecolmodel.2015.05.028>
- Vanderborght J, Couvreur V, Meunier F, Schnepf A, Vereecken H, Bouda M, Javaux M (2021) From hydraulic root architecture models to macroscopic representations of root hydraulics in soil water flow and land surface models. *Hydrol Earth Syst Sci* 25:4835–4860. <https://doi.org/10.5194/hess-25-4835-2021>
- Vetterlein D, Lippold E, Schreiter S, Phalempin M, Fahrenkamp T, Hochholdinger F, Marcon C, Tarkka M, Oburger E, Ahmed M, Javaux M, Schlüter S (2021) Experimental platforms for the investigation of spatiotemporal patterns in the rhizosphere-laboratory and field scale. *J Plant Nutr Soil Sci* 184:35–50. <https://doi.org/10.1002/jpln.202000079>
- Vetterlein D, Phalempin M, Lippold E, Schlüter S, Schreiter S, Ahmed MA, Carminati A, Duddek P, Jorda H, Bienert GP, Bienert MD, Tarkka M, Ganther M, Oburger E, Santangeli M, Javaux M, Vanderborght J (2022) Root hairs matter at field scale for maize shoot growth and nutrient uptake, but root trait plasticity is primarily triggered by texture and drought. *Plant Soil*. <https://doi.org/10.1007/s11104-022-05434-0>
- Zhou SW, Hu XT, Zhou ZJ, Wang WN, Ran H (2019) Improving water use efficiency of spring maize by adopting limited supplemental irrigation following sufficient pre-sowing irrigation in Northwest China. *Water* 11. <https://doi.org/10.3390/w11040802>

Publisher's note Springer Nature remains neutral with regard to jurisdictional claims in published maps and institutional affiliations.